11-8-2004

Modeling of QE, I-V Characteristics of MSM (Metal-Semiconductor-Metal) Mercuric Iodide Thin Films with MEDICI^{TM}

Vikram Rupavatharam
University of South Florida

Modeling of QE, I-V Characteristics of MSM (Metal-Semiconductor-Metal) Mercuric Iodide Thin Films with MEDICI™

by

Vikram Rupavatharam

A thesis submitted in partial fulfillment
of the requirements for the degree of
Master of Science in Electrical Engineering
Department of Electrical Engineering
College of Engineering
University of South Florida

Major Professor: Don L. Morel, Ph.D.
Christos S. Ferekides, Ph.D.
Yun. L. Chiou, Ph.D.

Date of Approval:
November 8, 2004

Keywords: HgI_2 , Photoconductors, Surface Recombination, Bulk Recombination, Parameter Extraction

ACKNOWLEDGMENTS

I have a deep feeling of gratitude to Dr.Don Morel, my Major Professor, for so many things that this could already easily fill this page of acknowledgements. He is the best professor I could have hoped for, full of optimism, ideas, understanding, and human warmth. I would like to offer my deep gratefulness to Dr. Chris Ferekides for his guidance and extremely helpful insights and also for accepting to be one of my committee members. My next appreciations are due, to Dr. Y.L. Chiou, who is also one of my committee members. I wish to acknowledge Prashanth Chegoor, Prince J.Simon who were part of Mercuric Iodide team at USF. They have been very helpful and cooperative in every way through out this work. Cheers to all my friends here in USA and in India, for not only making these years a very pleasant period to remember but also for being there whenever it matters. Finally, my parents, who always let me make my own decisions and stood by me in the past and the present.

TABLE OF CONTENTS

LIST OF TABLES

LIST OF FIGURES

MODELING OF QE, I-V CHARACTERISTICS OF MSM

(METAL-SEMICONDUCTOR-METAL)

MERCURIC IODIDE THIN FILMS WITH MEDICI™

Vikram Rupavatharam

ABSTRACT

Mercuric Iodide is the most promising of all semiconductor materials currently under investigation for use as radiation detectors at room temperature. While substantial studies have been conducted on single crystal HgI_2 , polycrystalline HgI_2 remains a comparatively less studied form.

The HgI_2 films are deposited on TEC-15 LOF glass with a Tin Oxide (SnO_2) coating which acts as the growth surface and front contact. The back contact, Palladium (Pd), is deposited by sputtering through a shadow mask. The films are circular in shape with an approximate diameter of 2.5 cm and thicknesses ranging from 50-600 μm. The film has seven contact points defined by Pd electrodes for spectral response(SR) and I-V measurements. Measurements were done on the film with a visible light source.

Numerical modeling helps us understand device properties and processes that take place in operation of the device. The focus of this work was to identify loss mechanisms in photoresponse, reveal fundamental device properties, and develop a quantitative device model for MSM HgI_2 thin films using the DC Device modeling simulation tool MEDICI™. The values for input parameters were chosen from literature, theory and

reasonable estimates. Comprehensive studies were performed to investigate the sensitivity of SR and light I-V characteristics to each input parameter. Surface&Bulk recombinations have been investigated in this thesis. A Single, homogeneous region with all possible combinations of carrier mobilities, surface and bulk recombination parameters was not able to explain completely the measured SR. A Two-region model with the first region (0-0.5) μm being surface&bulk recombination dominated, and the second (0.5-300) μm bulk recombination dominated, was able to match the complete measured SR of current devices. The key parameters determined from the simulations are the mobilities, bulk lifetimes and surface-recombination velocities at the front contact for both carriers. These are consistent with expectations based upon known single crystal properties.

CHAPTER 1

INTRODUCTION

Semiconductors are a group of materials having electrical conductivities between metals and insulators. The conductivity of these materials can be varied over orders of magnitude by changes in temperature, optical excitation, and impurity content. The column IV semiconductors, silicon and germanium are called elemental semiconductors because they are composed of single species of atoms. Compounds of column III and V atoms, as well as certain combinations from II and VI, and from IV, make up the compound semiconductors. Every solid has its own characteristic energy band structure. This variation in band structure is responsible for the wide range of electrical characteristics observed in various materials. Semiconductor materials at 0 K have basically the same structure as insulators. In metals, the bands either overlap or are only partially filled. Thus in metals, high electrical conductivity is due to the fact that electrons and empty energy states are intermixed within bands so that electrons can move freely under the influence of an electric field.

1.1 Direct & Indirect Band Gap Semiconductors

Matter, in general is composed of atoms which are made up of positively charged nuclei surrounded by just enough electrons to make the complete atoms electrically neutral. Distinctions between chemical properties of different materials arise because they are composed of different atoms. Distinctions between various phases (solid, liquid,

gaseous) of a given substance arise from differences in the strength with which its atoms are bound together. Atoms of solid-state materials have a sufficiently strong interaction that they cannot be treated as individual entities. Valence electrons are not attached (bound) to individual atoms; rather they belong to the systems of atoms as a whole. The energy bands can be thought of as the collection of the individual energy levels of electrons surrounding each atom.The wavefunctions of the individual electrons, however overlap with those of electrons confined to neighboring atoms.The Pauli Exclusion principle does not allow the electron energy levels to be the same so that one obtains a set of closely spaced energy levels, forming an energy band.The energy band model is crucial to any detailed treatment of semiconductor devices. Consider a valence band in ground state. The total crystal Momentum for this band is zero, as for every occupied k-state, there exists a corresponding filled state with opposite momentum. The top of valence band for most semiconductors occurs at k=0.The bottom of the conduction band in direct semiconductors occurs at k=0.Such semiconductors respond to external light, as the valence and conduction band edges are aligned in direct semiconductors. For indirect semiconductors, the bottom of the conduction band does not occur at k=0.An Indirect transition, involving a change in k, requires a change in momentum for the electron.Fig1.1 [1] shows the difference between direct and indirect semiconductors.

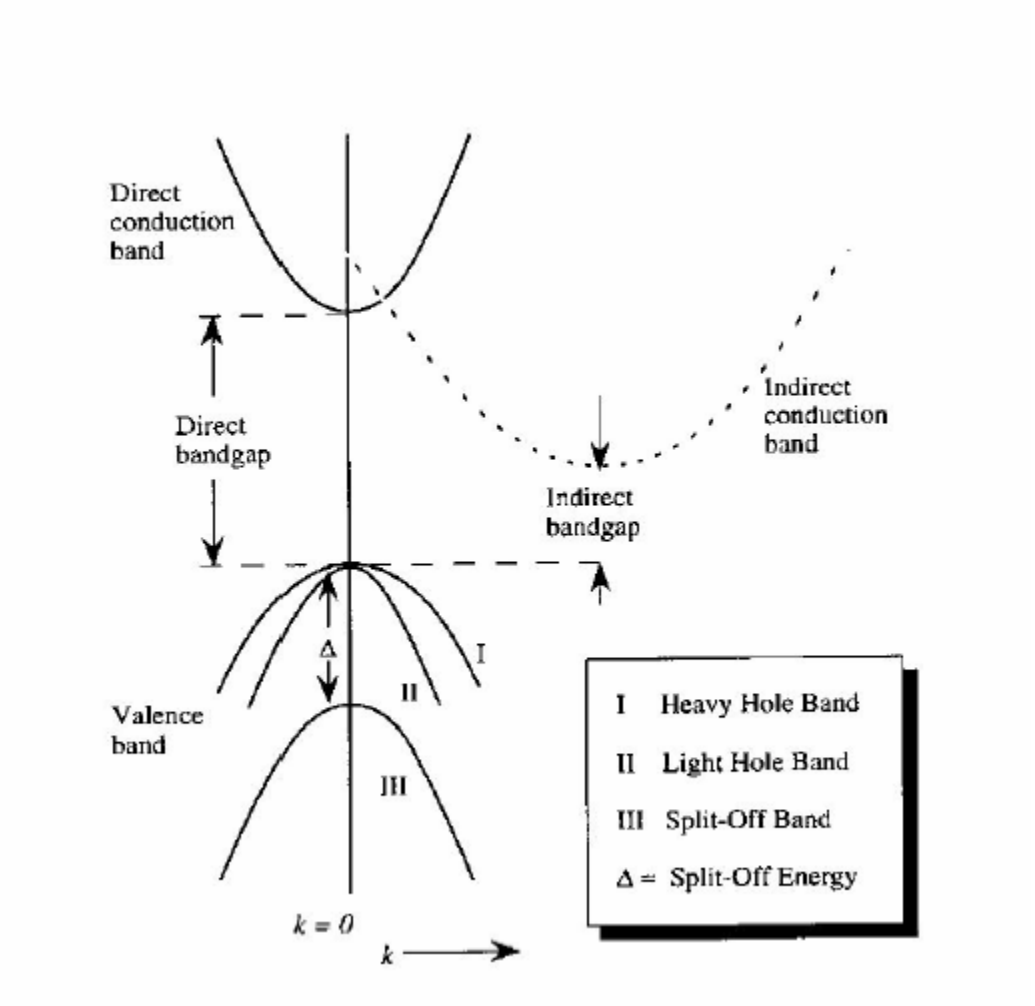

Figure 1.1 Band Structures of Direct and Indirect Band Gap Semiconductors

1.2 Fermi-Dirac Statistics

Fermi-Dirac statistics determines the statistical distribution of fermions over the energy states for a system in thermal equilibrium. Fermions are particles which are indistinguishable and obey the Pauli Exclusion Principle, i.e., that no two particles may occupy the same state at the same time.Electrons, protons and neutrons are all fermions. This theory explains the arrangement of electrons in orbitals around the nucleus of an atom and not collapsing into a common state. Energy bands consisting of a large number of closely spaced energy levels exist in crystalline materials. At a given temperature,

continuous thermal agitation results in excitation of electrons from valence band to conduction band and leaves behind an equal number of holes in valence band. The probability that an electron occupies an electronic state with energy E is given by Fermi-Dirac distribution function, given by

$$F(E) = \frac{1}{1 + \left(\exp(\frac{E - Ef}{kT} \right)} \tag{1.1}$$

Where E_F is the energy of Fermi-level. The Fermi energy is the energy at which the probability of occupation by an electron is exactly one-half. The energy band diagram is referred to a value known as the vacuum potential. The electron affinity, $q\chi$ is the energy required to remove an electron from the conduction band to the vacuum potential.

1.3 Carrier Transport

At temperatures above 0K, electrons within a piece of semiconductor have finite thermal energy (kT) and therefore possess finite velocity. This velocity is known as the thermal velocity of the electron, $V_{th.}$ Because the motion of electrons under thermal excitation is a random process, the average velocity of the electrons is zero and there is no net displacement of electrons over time. A motion of free carriers in a semiconductor leads to a current.This motion can be caused by an electric field (Drift).In addition, carriers also move from regions where the carrier density is high to regions where the carrier density is low (Diffusion), which is due to the thermal energy and the associated random motion of carriers. The total current in a semiconductor equals the sum of drift and diffusion currents. As one applies an electric field to a semiconductor,the electrostatic force causes the carriers to first accelerate and then reach a constant average velocity,as the carriers scatter due to impurities and lattice vibrations.The ratio of velocity

to the applied field is called the mobility.Carriers within a semiconductor crystal move as if they are free particles which are not affected by presence of the atoms in the material, except for the fact that it effectively changes the mass of particle.The carriers even move when no electric field is applied because of the thermal energy associated with the particles.At room temperature,the thermal velocity of electrons in bulk semiconductors is about 10^7 cm s^{-1} .The carriers move through the semiconductor until a collision occurs.These collisions cause an abrupt change in the carrier velocity and energy at the time of collision.The resulting carrier motion is semi-random due to frequent changes in direction and velocity.Carrier transport in a semiconductor in the presence of an applied field can also be visualized as being semi-random except that in addition,the individual carriers also accelerate between collisions.The carrier acceleration follows Newton's law. The net effect of the collisions is that the carriers on average do not accelerate, but rather quickly reach a constant velocity. Mobility is a physical constant that describes the ease with which an electron or hole can move through a material. The mobility is a function of temperature as well as the electric field. The mobility of electrons and holes is determined by the charge, effective mass, and finally, the relaxation time of current, or average time between the scatterings of the carriers. Scattering by ionized impurities and Scattering by mechanical vibrations of the crystal are the two most significant modes.

1.4 Carrier Recombination

The behavior of carriers in semiconductors has been studied extensively due to its importance in determining the operation of semiconductor devices. However, there are

three distinct processes which are considered fundamental and from which the operation of all semiconductor devices can be described. They are that of carrier drift, diffusion and recombination/generation.

Recombination within semiconductor devices usually occurs through a number of simultaneous processes. These processes can be broadly classified as intrinsic or extrinsic in nature [28]. Intrinsic processes are unavoidable properties of the semiconductor material and include radiative recombination [29] and Coulomb-enhanced Auger recombination [30].Extrinsic processes relate to defects (impurities, crystallographic imperfections, etc) within the material or at its surface and include Shockley-Read-Hall bulk [31] and surface recombination [32].

Three fundamental recombination mechanisms that occur in semiconductors are Radiative recombination, Auger recombination and Recombination through defects in the bandgap. Other recombination processes within devices can generally be viewed as a manifestation of these three fundamental mechanisms. The surface of a semiconductor represents an abrupt discontinuity in its otherwise uniform crystal structure. The high number of dangling bonds creates a large density of defects throughout the bandgap. Therefore, surface recombination is a particular case of "Recombination through defects in bandgap" [25].

The most relevant parameter for characterizing carrier recombination in a semiconductor is the recombination lifetime. Schroder [25] has pointed out that the "Recombination lifetime is a property of the carriers within the semiconductor, rather than a property of the semiconductor itself. As such, it is a weighted average across all the carriers, whose individual behaviors may be influenced by different factors, including

surfaces, bulk defects and the density of carriers, besides the fundamental properties of the semiconductor material"[25]. Recombination lifetime represents a number of specific recombination mechanisms occurring simultaneously within the bulk and at the surfaces. SRH recombination can occur either at surface as a result of surface states or through bulk defects or impurities.

1.4.1 Bulk Recombination

The band diagram of a perfect single crystal semiconductor consists of a valence band and a conduction band separated by a band gap. When the periodicity of the single crystal is perturbed by foreign atoms or crystal defects, discrete energy levels are introduced into the band gap, shown by E_T lines. Each line represents one such defect with energy E_T . Such defects are commonly called Generation-Recombination (G-R) centers or traps. The presence of defects within a semiconductor crystal, be they from impurities or crystallographic imperfections such as dislocations, produces discrete energy levels within the bandgap. These defect levels, also known as traps can involve in recombination through a two-step process whereby a free electron from the conduction band first goes to the defect level and then jumps to the valence band where it recombines with a hole. The dynamics of this recombination process were first analyzed by Shockley and Read [26] and Hall [27]. It should be noted that these recombination centers can act also as traps (or even solely as traps), in which a carrier is captured and subsequently injected back into the band from which it came. Although not contributing directly to recombination, trapping, by changing the free carrier concentrations, can nevertheless impact heavily on the overall carrier dynamics. The result is a pair of coupled (meaning the variables of interest are defined in terms of one another), first order differential

equations in Δn and Δp for the electron and hole lifetimes.

$$g_e - \frac{d\delta n}{dt} = \frac{\nabla n}{\tau_n} = \frac{1}{\tau_{n0}}\left[\left(\frac{(n_0 + n_1 + \nabla n)(\nabla n - \nabla p))}{N}\right) + \frac{\nabla n n_1}{n_0 + n_1}\right] \quad (1.2)$$

$$g_e - \frac{d\delta p}{dt} = \frac{\nabla p}{\tau p} = \frac{1}{\tau_{p0}}\left[\left(\frac{(p_0 + p_1 + \nabla p)(\nabla p - \nabla n))}{N}\right) + \frac{\nabla p p_1}{p_0 + p_1}\right] \quad (1.3)$$

Here g_e is the generation rate arising from external illumination and n_0 and p_0 are the electron and hole concentrations in thermal equilibrium. τ_{n0} and τ_{p0} are sometimes known as the fundamental electron and hole lifetimes, and are related to the carrier thermal velocity V_{th}, the recombination centre density N and the capture cross-sections σ_n and σ_p of the specific centre in question:

$$\tau_{p0} = \frac{1}{N v_{th} \sigma_p} \quad (1.4)$$

$$\tau_{n0} = \frac{1}{N v_{th} \sigma_n} \quad (1.5)$$

The statistical factors n_1 and p_1 in Equations 1.2 & 1.3 are the electron and hole densities when the Fermi level coincides with the recombination centre energy E_T.

$$n_1 = N_c \exp\left(\frac{E_T - E_C}{kT}\right) \quad (1.6)$$

$$p_1 = N_V \exp\left(\frac{E_C - E_G - E_T}{kT}\right) \quad (1.7)$$

Where N_C and Nv are the effective densities of states at the conduction and valence band edges and E_C and E_G the conduction band and band-gap energies.

The SRH lifetime depends inversely on the density of recombination centers and capture cross sections, but does not depend directly on the energy level of the impurity. It does depend indirectly on the energy level, because the capture cross section tends to be highest for impurities with near the center of the bandgap and lowest for near the conduction or valence band.

"We know that electrons move randomly at their thermal velocity V_{th} and that G-R centers remain immobile in the lattice. Nevertheless, it is helpful for the discussion to change the frame of reference by letting the electrons be immobile and the G-R centers move at velocity V_{th} .The centers then sweep out a volume per unit time of σV_{th} and those electrons that find themselves in that volume have a very high probability of being captured" [25]. Capture cross-sections vary widely, depending on whether the center is neutral or negatively or positively charged. In general, a center with a negative or repulsive charge has a smaller electron capture cross-section than the one that is neutral or attractively charged. Neutral capture cross-sections are on the order of 10^{-15} cm^2.

The capture cross-section is a measure of how close to a trap center a carrier has to come to get captured. For Electron trap, $\sigma_n >> \sigma_p$, for hole trap, $\sigma_n << \sigma_p$. Traps behave as recombination centers when $\sigma_n = \sigma_p$ where σ_n is the capture cross-section for a free electron by a center occupied by a hole. σ_p is the capture cross-section for a free hole by a center occupied by an electron. For the state to be considered as a trapping center or as a recombination center depends on the relative magnitudes of:

1. The probability of thermal freeing of the trapped carrier
2. The probability of recombination with the carrier of opposite sign occurring at the center before the thermal freeing of the carrier trapped first.

The recombination center density varies from $10^{12}\,cm^{-3}$ (for high purity and good quality materials) to $10^{18}\,cm^{-3}$. Similarly capture cross-section also varies from $10^{-12}\,cm^{-2}$ to $10^{-20}\,cm^{-2}$.

1.4.2 Surface Recombination

The major cause for change in semiconductor device parameters as a function of time is the changes that occur at the surfaces. The termination of the crystal at a surface represents a discontinuity in periodic potential, and Shockley has suggested that this "Interruption results in extra allowed states for electrons within the forbidden band". [2]. It is supposed that the energy gap is constant all the way to the surface, and surface effects are represented as electronic states in the forbidden band. The surface states may be either donors or acceptors; the actual type of state in many cases can be inferred only indirectly. One of the fundamental phenomena associated with surface states is the bending of bands near the semiconductor surface. If the surface states are predominantly acceptors, the surface tends to become negative, thereby attracting holes or repelling electrons. The surface states that hold charge and act as donors and acceptors can also act as recombination centers.

Surface recombination is a special case of SRH recombination in which the localized states occur at the surface. Unlike bulk SRH centers, these states do not usually occupy a single energy level, but rather form a set of states distributed across the band-gap. It has to be reformulated in terms of recombination events per unit surface area, rather than per unit volume. Surface recombination analysis is performed in terms of surface recombination velocities (SRV) instead of lifetimes, however, the principles are identical to bulk SRH recombination.

The model is changed slightly to allow for the possibility that the "Fermi level at the surface is not at the same energy relative to the band edges as in the bulk, net charge at the surface can cause the energy of the band edges at the surface to be shifted from the bulk, an effect known as band-bending" [32].

For a single defect at the surface, the rate of surface recombination, U_s is given by

$$U_S = \frac{n_s p_s - n_i * n_i}{\frac{n_s + n_1}{S_{p0}} + \frac{p_s + p_1}{S_{n0}}} \tag{1.8}$$

Where n_s and p_s are the concentrations of electrons and holes at the surface, and S_{n0} and S_{p0} are related to the density of surface states per unit area, N_{ts} and the capture cross-sections, σ_p and σ_n, for the specific defect.

$$S_{n0} = \sigma_n v_{th} N_{ts} \tag{1.9}$$

$$S_{p0} = \sigma_p v_{th} N_{ts} \tag{1.10}$$

It is the surface recombination velocity, S, that is typically used for quantifying surface recombination processes. If the energy levels of the band edges are shifted so that the energy of the conduction band edge is higher at the surface than in the bulk by energy ψ,the carrier concentrations at the surface can be approximated by,

$$n_s = n \exp\left(\frac{-\Psi}{kT}\right) \tag{1.11}$$

$$p_s = p \exp\left(\frac{\Psi}{kT}\right) \tag{1.12}$$

For a given excess carrier concentration, a higher surface recombination velocity, V_s results in a higher rate of recombination.

$$v_s = \sigma_s N_{ts} v_{th} \exp(\frac{-\Psi}{kT}) \qquad (1.13)$$

The effect of the electric fields in the surface space charge layer is included in the surface recombination velocity via (1.9) [34].The surface recombination velocity depends both on cross sections for electron and hole capture by defects and on the potential difference between the surface and the bulk of the sample [35].

Trapping is the mechanism by which some of the excess e^- h^+ pairs, originally created in equal densities, are trapped temporarily on impurities. Those electrons captured in traps can be subsequently emitted back to the conduction band by thermal emission. Surface recombination is a more complicated process than bulk recombination, because it depends not only on the density of surface states or interface traps, but also on the state of the surface [36].

The presence of charged traps at the surface results in formation of an electric field which repels (or attracts) the carriers carrying the same (opposite) charges as the surface. Donor traps are positively charged when empty, neutral when filled. Acceptor traps are negatively charged when filled and neutral when empty. For cases, where hole and electron densities at the surface are comparable, two different surface recombination velocities are used, one for electrons and the other for holes. The usual assumption is that surface recombination velocity is proportional to the trap density. In fact, "surface recombination velocity for electrons is proportional to the density of empty traps, whereas for holes, proportional to the density of filled traps". [37]

CHAPTER 2

SEMICONDUCTORS-OPTICAL RESPONSE

2.1 Optical Absorption in Semiconductors

"Radiation primarily interacts with bound electrons" [19]. For example, a silicon atom contains 14 electrons in a sphere with a radius of 0.12 nm that presents a geometrical cross section of $4.5*10^{-20}$ m^2 .The nucleus at the center of the sphere has a radius of 3.6 fm with a geometrical cross section of $4.1*10^{-29}$ m^2 .The geometrical probability to strike the electrons in an atom is something like 9 orders of magnitude higher than to strike the nucleus. There are basically three processes for interaction between a photon and an electron in a solid: absorption, spontaneous emission and stimulated emission. Absorption of a photon occurs when the radiation incident on semiconductor imparts energy to an electron. If the photon energy is greater than or equal to the bandgap, an electron-hole pair is generated and the excess energy is dissipated as heat .Thus, as a beam of photons propagates through any material, the intensity of the beam will decrease as the photons that interact are removed but the energy of all the non-interacting photons will remain constant. Low energy photons will interact only once and give rise to a single electron hole pair, energetic photons can interact several times and give rise to a few electron hole pairs [19]. The energy of the non-interacting photons remains constant so that the "Probability that a photon will interact in a fixed thickness of

material will also remain constant regardless of the photon energy" [19]. This leads to an exponential attenuation of electromagnetic radiation, which is called The Beer-Lambert Law. Each of the photons that interacts with an atom via any one of the mechanisms will be lost from the beam. When the photon interacts with a bound electron, the photon can be completely absorbed and the electron emerges with a kinetic energy that corresponds to a photon energy hυ,minus the electron binding energy,KE = hυ-BE. The cross section or probability of the photoelectric effect is on the order of a square of atomic size for photons in the KeV region and decreases rapidly with increasing photon energy. The cross section has a strong dependence on the atomic number of the absorbing material. As an example, the heavy element lead(Z=82) has K,L,M(principal quantum numbers n=1,2,3) binding energies of approximately 88,15,and 3 KeV respectively, which provide strong photoelectric absorption for photons in this energy region.

The photon absorption for a particular wavelength is dependant on a parameter called the absorption co-efficient (α). This parameter serves as a quantitative measure in identifying strong, uniform absorption of incident radiation in a semiconductor. The photon density diminishes from the incident surface into the bulk of semiconductor as:

$$N(x) = N_0 \exp(-\alpha x) \quad (2.1)$$

N_o, incident photon flux.

The photon density distribution in the specimen depends on α and on the thickness of the specimen. The photon density at the back side of the specimen, of thickness d is equal to

$$N_1 = N_0 \exp(-\alpha d). \text{ From equation (2.1)} \quad (2.2)$$

The number of photons absorbed in the specimen (per unit area) is the following:

$$N_2 = N_0 - N_1 = N_0 (1 - \exp(-\alpha d)) \quad (2.3)$$

When $\alpha d << 1$, i.e., if either α is small or the specimen is thin, then $N_1 = N_0$ .The distribution of photon flux is practically uniform. Almost all the photons which got into the specimen fly out of it, unabsorbed.

When $\alpha d = 1$, an appreciable part of incident flux (63%) is absorbed in the specimen.

When $\alpha d >> 1$ the incident flux is absorbed in a narrow region next to surface.

2.2 Semiconductor Photon Detectors

A photodetector is a device that measures photon flux or optical power by converting the energy of the absorbed photons into a measurable form. Photographic film is probably the most ubiquitous of photodetectors.Two principal classes of photodetectors in common use are: thermal detectors and photoelectric detectors. The operation of photoelectric detectors is based on the photoeffect, in which the absorption of photons by some materials results directly in an electronic transition to a higher level and the generation of mobile charge carriers. Under the effect of an electric field, these carriers move and produce a measurable current. The photoeffect takes two forms: external and internal. The former process involves photoelectric emission, in which the photogenerated electrons escape from the material as free electrons. In the latter process, photoconductivity, the excited carriers remain within the material, and serve to increase its conductivity.

2.3 Photoconductivity

Photoconductivity is an important property of semiconductors by means of which the bulk conductivity of the sample changes due to incident radiation. Photoconduction, as the name suggests, includes the generation and recombination of charge carriers and their transport to the electrodes. “Obviously charge carrier statistics, effects of electrodes,

and several mechanisms of recombination are involved in conduction" [5]. Every mechanism is a complicated one, and therefore photoconductivity in general is a very complex process. To make an adequate or proper contact to photoconductors is not a simple problem and there is not an easy solution. This is because the contact material and contact techniques depend on the semiconductor itself. Surface preparation is important not only for achieving good metal-semiconductor contacts but also for avoiding or reducing the effects of surface states. The choice of contact material and method of making the contact depend upon the specific requirements. Some types of contacts are desirable for one purpose but, seriously harmful for other purposes. This is also true of the geometry of contacts. For high-speed photoconducting sensors, Schottky barrier type contacts are desirable to increase the collection efficiency of the electrons and to improve the speed of devices [4].Criteria for eliminating the effects of neutral contacts and their pertinent details have been discussed extensively [5].

"Photoconductivity is one of a few topics where experimental setup, contact configuration, preparation of the sample, and sample thickness play a crucial role in the output and in the analysis of the results. The overall shape of the spectral response curve may be considered to trace faithfully the physical mechanisms (optical absorption and carrier transport) of the detector, but the magnitude of the photoresponse and the transient properties such as speed and lifetime of the charge carriers may be strongly influenced by experimental details that may appear to be unimportant" [5]. The role of contacts (even unilluminated), independent of their nature (blocking, injecting, or neutral) is also a complex issue. While the contacts are made between metals and semiconductors depending upon the workfunction, there is a flow of charge carriers from the higher to

lower Fermi level to equalize the Fermi level at the contact. In this process, electrons can transfer from the semiconductor to metal, resulting in a depletion region in the semiconductor. This gives rise to perturbation of the band at the metal-semiconductor interface. The flow of charge carriers is influenced by the length of the depletion region and the amount of perturbation at the interface.

When the regions near the contacts are illuminated, quasi-fermi levels for electrons and holes move relative to the Fermi level of the metal. If the illumination is intense, the movement of the Fermi level may be large enough to change the nature of contact and hence change its overall properties.

2.4 Photoconductors

Semiconductor light detectors can be divided into 2 major categories: junction and bulk effect devices. Junction devices, when operated in the photoconductive mode, utilize the reverse characteristics of a p-n junction. Under reverse bias, a p-n junction acts as a light controlled source. Output is proportional to incident illumination and is relatively independent of applied voltage. In contrast, bulk effect photoconductors have no junction. The bulk resistivity decreases with increasing illumination, allowing more photocurrent to flow. This resistive characteristic gives the bulk effect photoconductors the unique quality that signal current from the detector can be varied over a wide range by adjusting the applied voltage. Photoconductive detectors can operate through either intrinsic or extrinsic photoconductivity. Photons with energy, $h\upsilon > E_g$ excite electrons across the bandgap. The electron-hole pair that is thereby created for each photon absorbed leads to an increase in conductivity.

Semiconductors with small bandgaps respond to long wavelength radiation but

must be cooled accordingly, otherwise thermally excited electrons swamp any small photoconductivity effects. The following table lists commonly available intrinsic photoconductors, with their usual operating temperatures [16].

Table 2.1: Intrinsic Photoconductors Vs Operating Temperatures and Energy Gaps

Semiconductor	T(K)	Eg
Cds	295	2.4
CdSe	295	1.8
Si	295	1.12
Ge	295	0.67
PbS	295	0.42
PbS	195	0.35
PbS	77	0.32
PbSe	295	0.25
InSb	77	0.22

The simplest bulk effect photo detector is an intrinsic semiconductor with contacts at two ends. This configuration was used for our research. Generally most research on photoconductors has assumed that light is incident on the bulk of the semiconductor perpendicular to the applied electric field. This configuration is shown in figure 2.1.

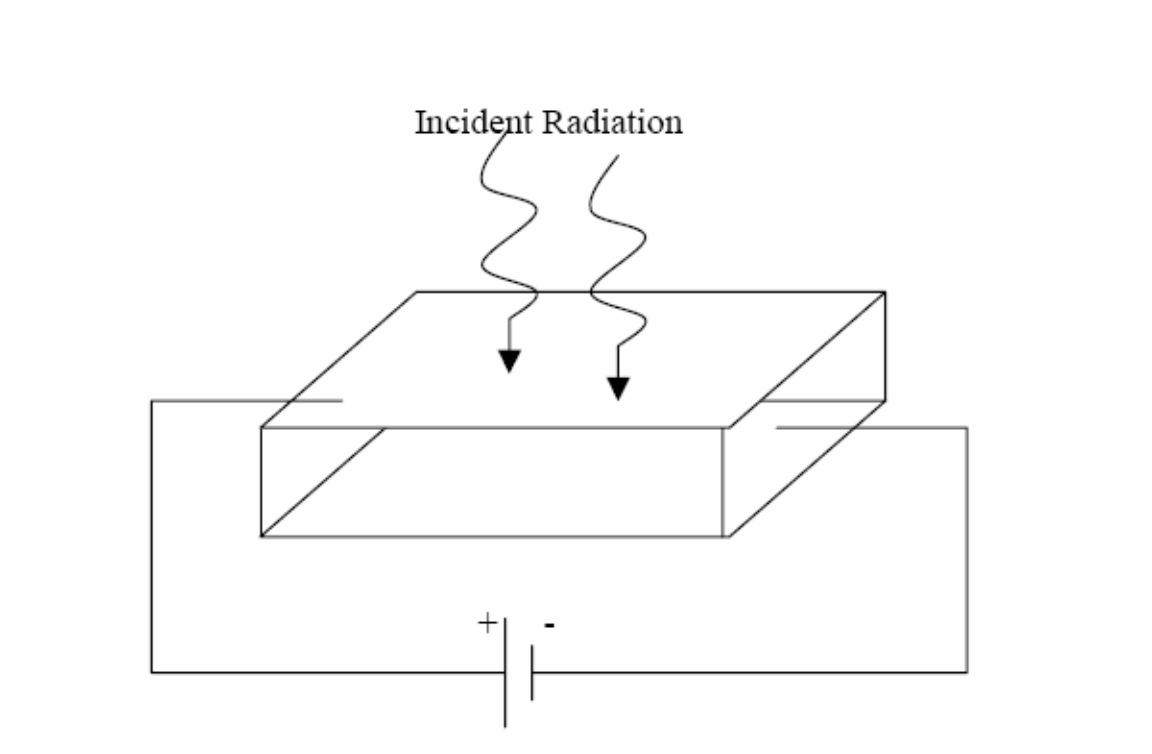

Figure 2.1: Geometry of Bulk Photoconductor [38]

Another possible configuration is to make one of the contact electrodes transparent. The detector is then illuminated through the transparent electrode. The photogeneration now takes place along the applied field. This kind of setup is very useful in studying thin film photoconductors which we used for our research.

2.5 Spectral Response

The photocurrent produced by a given level of incident light varies with the wavelength. This relation between the photoelectric sensitivity and wavelength is referred to as the spectral response characteristic and is expressed in terms of photosensitivity, quantum efficiency (QE), etc.

There are two kinds of QE, internal and external. External QE at each wavelength is a dimensionless parameter given by the ratio of number of electron hole pairs, which exit the device and number of incident photons at each wavelength. Internal QE at each

wavelength is a dimensionless parameter given by the ratio of number of electron hole pairs, which exit the device and number of absorbed photons at each wavelength. Device losses measured by external QE can be optical, due to reflection, transmission and absorption, or electronic, due to recombination losses. Quantum efficiency (QE) measurements are valuable to characterize the photocurrent and are commonly used to determine the losses responsible for reducing the measured photocurrent from the maximum achievable photocurrent. Because α varies strongly with λ, use of different λ from 400-570 nm produces absorption depths $1/\alpha$ which vary from 0.03 µm to 15 µm in HgI_2 . "This allows the distribution of photogenerated carriers to either extend well into the bulk, or to be highly localized at the Surface" [20]. The fraction of carriers which will be collected by the field at the front depends strongly upon the bulk life time and surface recombination velocity. "This functional dependence allows recombinative parameters to be extracted from the spectral dependence of the photocurrent" [20].

CHAPTER 3

MERCURIC IODIDE

Semiconductor materials can further be classified by categories such as size, content and complexity. For instance, size distinguishes thin film semiconductors from bulk semiconductor materials. Due to surface and quantum-confinement effects, the characteristics can be modified significantly [20]. In addition, a material can be designated as either monatomic or compound, based on atomic composition. Compound semiconductors can be further categorized as binary, ternary or quaternary according to the number of composite elements incorporated. These may be formed from semiconducting or non-semiconducting elements. The particular advantage of these compounds is that they provide the device engineer with a wide range of energy gaps and mobilities, so that materials are available with properties which exactly match specific requirements.

Mercuric iodide is a II-VI compound semiconductor having a phase transition from low-temperature tetragonal form to the high-temperature orthorhombic form. This transformation occurs at 400^0 K, changing the color of the material from red to yellow .Its optical properties especially the red form, have been investigated for several years .The increasing interest for the development of gamma ray detectors has necessitated the establishment of the electrical properties of this material.

3.1 Literature Review

An intense research and development effort in wide bandgap semiconductors has been motivated by the need for lightweight, handheld, portable nuclear radiation spectrometers capable of operating at room temperatures. The only single chemical element semiconductor with wide bandgap is Diamond. The bandgap of diamond is 5.5 eV. Unfortunately, carbon is a light element and a lot of it is needed to stop typical x-rays. This leaves us with compound semiconductors. A wide range of compound semiconductors are at various stages of development for this application. Among these materials, Mercuric iodide (HgI_2) and CdTe are in the most advanced state of development. The most important criteria upon which one bases the selection of semiconductor material to serve as a spectrometer include "Energy gap (E_g), average atomic number Z, charge transport properties (mobility, lifetime), electrical resistivity, and homogeneity of material in terms of purity, stoichiometry, and absence of structural defects" [6]. A large E_g (>1.4eV) will prevent thermal generation of carriers and thus ensure a low dark current.However, if E_g is (>3.0eV) the energy required for electron-hole formation will be increased to the point of decreasing the detector efficiency [6]. Highly uniform material is critical, since this allows for fabrication of large volume detectors that provide large interaction volume and high efficiency. High resistivity is generally required (>10^7 Ωcm) so that material can sustain large electric fields (>10^4 V/cm) and maintain low dark current.Finally, mobility-lifetime products should be high to allow for charge transport across the detector.

Mercuric Iodide has been a subject of interest for more than 30 years owing to its efficiency as a room temperature detector for high energy radiation(X and γ-rays).This

property was discovered by Chepur in 1956[7], however it was the work of Wilig in 1971[8] which actually triggered further investigations on this difficult material. Elemental semiconductors (Si and Ge) have to be cooled down to liquid nitrogen temperature when used as nuclear detectors. Room temperature operation combined with a high attenuation and good energy resolution of Mercuric Iodide open the way to miniaturization and portability of detectors and spectrometers. Its wide bandgap (2.13 ev) in conjunction with high atomic numbers of its constituent atoms (Z=80 and 53 for Hg and I, respectively) makes it an attractive material.Infact, commercial battery operated, field portable x-ray fluorescence (XRF) systems have been available for many years [9].The performance of these truly portable XRF systems is the first to rival that of laboratory XRF systems based on Si (Li) detectors. Since photoelectric absorption varies as Z^5, the specific sensitivity of HgI_2 is about 100 times greater than Ge for energies<200 KeV. HgI_2 has a high photon absorption coefficient, wide band gap of 2.13 eV and a low hole-electron pair creation energy of 4.2 eV at 300K[10].However, the "Development of HgI_2 detectors has been somewhat hampered by the problems encountered in controlling residual impurities,stoichiometry and physical defects in crystals" [18]. The presence of bulk imperfections as well as the high surface reactivity of HgI_2 have detrimental effects on device stability, both during detector operation (short term and storage (long term). "A better control of the surface properties and the use of convenient coating procedures have greatly improved the long term stability" [37]. In contrast, the short term instability, which is mainly related to bulk properties, still remains a great concern.

Actually,measurements of the I-V characteristics of HgI_2 –based devices appear often not to be reproducible as the results depend strongly on the experimental

procedure.Not only the voltage increment and time left before increasing the voltage,but also the time during which the sample has been left unbiased before the actual measurement play an important role[11]. "There are atleast two well defined fronts to investigate mercuric iodide: fundamental issues, such as the electronic and optical properties, and the growth issues, such as defect and impurity defects" [39]. Applications have been found in geological explorations, marine mineral analysis, environment pollution monitoring, industrial material quality assurance, and space explorations [12].

3.2 Crystal Structure

The known polymorphic forms of mercuric iodide are: red α, yellow β and a metastable orange phase [13].α-HgI_2 is tetragonal. Figure 3.1 shows the unit cell of α-HgI_2. Two Hg atoms are located at positions (0,0,0) and (1/2,1/2,1/2) and four I atoms at (0,1/2,u),(1/2,0,u),(0,1/2,1/2 + u) and (1/2,0,1/2-u) with u=1.78A^0 .One mercury atom surrounded by four iodine atoms form the co-ordination unit of crystal.The slightly distorted tetrahedra are linked by the corners to form sheets parallel to the (001) plane. Each sheet consists of 3 layers of atoms (Iodine-Mercury-Iodine).Mercury atoms occupy ¼ of the tetrahedrally coordinated voids of the iodine sub-lattice in each sheet.Vander waals bonding forces keep the adjacent sheets together. The Hg-I distance within the tetrahedra is 2.783 A^0 , whereas the shortest I-I distance of 4.142 A^0 is found between neighboring layers of the tetrahedra. No other compound crystallizes in the manner as HgI_2 does [14].The structure is unique to HgI_2.

Table 3.1: Crystallographic Data of HgI_2 [38]

Parameter	α- HgI_2
Lattice constant a (A^0)	4.361

Table 3.1 (Continued)

Lattice constant b (A^0)	-
Lattice constant c (A^0)	12.450

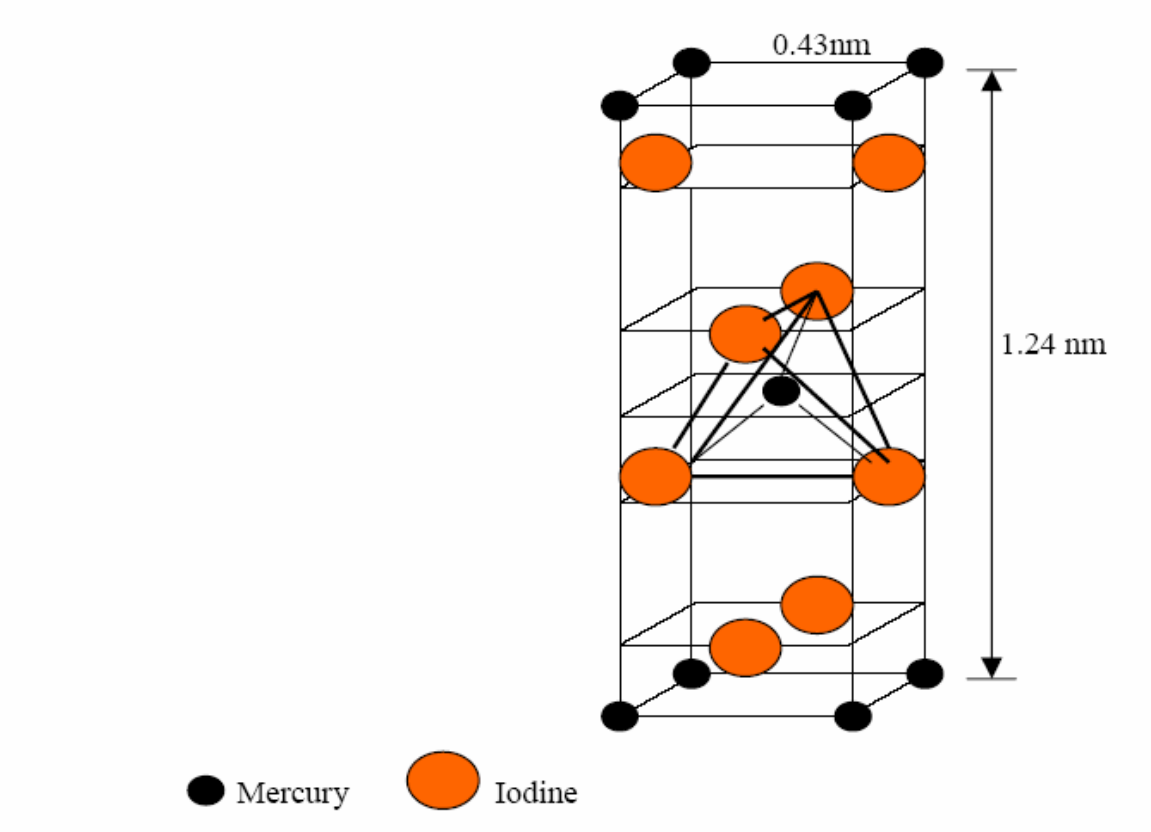

Figure 3.1: Elemental Cell of Tetragonal α – HgI_2 [38]

The tetragonal lattice shown in Figure 3.1 exists below 130^0 C.On heating above this temperature, it transforms to the β phase, which has an orthorhombic lattice and has a bandgap of 2.5eV.When the β phase is cooled, it transforms back into α phase. This transformation is destructive in nature which requires HgI_2 to be usually operated below 130^0 C.

CHAPTER 4

INTRODUCTION TO MEDICI™

4.1 Previous Work on Modeling

The first attempt to model the device performance of HgI_2 films was done with AMPS, a first principles simulation code from Penn State University [41]. "When representative values were used for fundamental parameters to perform simulation using AMPS, generated current-voltage and quantum efficiency spectral response plots from simulation were in agreement with the experimental results from single-crystal reference devices" [15]. "Further insights through simulation suggested that electron transport properties suffered relative to the hole properties in thin films" [15]. Simulations with 50 V bias, the bias applied for measurements on HgI_2 thin films, can't be done with AMPS, as AMPS is limited by low applied voltage and low wavelength resolution. MEDICI™ ,a commercial semiconductor-device simulator, developed by TMA [40] does not have such limitations on the bias that can be applied on the device. This was the main reason MEDICI™ was chosen for modeling of HgI_2 thin films.

The earlier work done with MEDICI™ in modeling HgI_2 thin films was to obtain carrier transport parameters and light absorption profiles for polycrystalline HgI_2 thin films [38]. This was done by comparing the simulated spectral response and light I-V characteristics with the corresponding measurements done on thin films. This thesis attempts to go into more details of modeling of thin films with MEDICI™ .

MEDICI™ is an industry-standard device simulation tool that predicts electrical, thermal and optical characteristics of arbitrary two-dimensional structures under user-specified operating conditions. A wide variety of devices can be modeled in 1 and 2-D including MOSFETs, BJTs, HBTs, power devices, photodetectors and LEDs. With the most advanced physical models available, MEDICI allows device design to be optimized for best performance without fabrication, eliminating the need for costly experiments.

4.2 Analyzing Devices

MEDICI™ does not require the user to specify equations in the program to describe the semiconductor device physics. Instead, it asks the user to specify the size and structure of the device, the desired model, the locations of the contacts within the device structure, and also any special boundary conditions or physical models to be used in the simulation. It models the two dimensional distributions of potential and carrier concentrations in a device. The primary function of Medici is to solve three partial differential equations: Poisson's Equation, Continuity Equations and the Boltzmann transport equation, self-consistently for the electrostatic potential, ψ, and for the electron and hole concentrations, n and p respectively. MEDICI can be used to study devices under transient operating conditions as well.

4.3 MEDICI Grid

MEDICI uses a non-uniform triangular simulation grid and can model arbitrary device geometries. The simulation grid can also be refined automatically during the solution process. The correct allocation of the grid is a crucial issue in device simulation. As different parts of a device have very different electrical and optical behavior, it is usually necessary to allocate a fine grid in some regions and a coarse grid in others. The

differential equations to be solved for each simulation are discretized in a simulation grid, as described in [40].The resulting set of algebraic equations is coupled and nonlinear that must be solved by a nonlinear iteration method from an initial guess. Two methods are widely used for this- Gummel's and Newton's [40].

4.4 Physical Models in MEDICI

A number of physical models for recombination, photogeneration, mobility and lifetime are incorporated into the program for accurate simulations. MEDICI also incorporates both Boltzmann and Fermi-Dirac statistics.

4.5 Modules in MEDICI

The MEDICI Optical Device Advanced Application Module (OD-AAM) is used to model propagation of light inside and outside a device. It allows calculation of spectral response of the optical devices in steady-state or in transient modes. One of the major capabilities of OD-AAM is the treatment of the stack of multiple layers as a single film to consider interference effects. The Trapped charge Advanced Application Module (TC-AAM) allows detailed analysis of semiconductor devices containing traps. It allows simulation of carrier trapping and de-trapping mechanisms within semiconductor materials which are important in deep trap levels. For the analysis of traps the energy gap is divided in up to 50 discrete levels. The recombination and trapping processes are then analyzed at each level.

MEDICI helps user to extract the following information from device structures.

1. Determine I-V characteristics and current density distributions.
2. Understand internal device operation through simulation of the electrostatic field, carrier concentrations, current density.

3. Determine Spectral response and photocurrents under any voltage bias.

4.6 Co-ordinate Systems

The program gives a choice of Cartesian or Cylindrical coordinate systems. MEDICI is a two-dimensional simulator, so regardless of the coordinate system used; simulations are performed in only two of the three space dimensions. When using the Cartesian system, simulations are performed in the xy- plane. The device behavior is assumed to be identical for all values of z. For this reason, terminal currents are expressed in units of Amps/micron.

4.7 Execution of MEDICI

The program is directed via input statements. These statements may appear in a command input file or may be entered interactively from the terminal. Each statement consists of a statement name followed by a list of parameter names and values. A MESH statement is used to initiate the generation of a device structure. A rectangular mesh can be a very effective solution mesh. After giving a proper grid structure in the X & Y directions, the contacts have to be placed and named which is done by the ELECTRODE statement. As there is no material library for HgI_2 in MEDICI, the user has to give the material properties accordingly. For the optical analysis, the source of radiation has to be given which is a spectral source for Spectral response and monochromatic for I-V characteristics at a single wavelength.

The advantage of MEDICI^{TM} over other simulation tools is user control over the physics used in the calculations. It is easier to check the equations used by the program when simulating the device. It is also easy to change the material properties in an easy and consistent way.

CHAPTER 5

SIMULATION RESULTS

5.1 Input Data

Input parameters for the simulation are selected based on literature values, theory, and in some cases, reasonable estimates. Types of parameters required before any MEDICI™ simulation can be started:

1. Mesh which represents the device structure, 2 D Cartesian co-ordinate system was used for this thesis.
2. Material properties i.e., electrical and optical properties of each layer, including front and back contact
3. Selection of models, i.e., model type for carrier statistics, recombination statistics. Fermi-Dirac statistics was used for this thesis.
4. Numerical-solution method: The Newton-Raphson method was used for this thesis.

Material properties (used in simulation):

Table 5.1: Basic Material Properties of HgI_2

Width	300 µm
Permittivity	11
Band gap	2.13 eV
Effective density of states N_C	2.0e19 cm^{-3}

Table 5.1(Continued)

Effective density of states N_V	2.0e19 cm^{-3}
Electron affinity	4 eV
Refractive index	2.8

As there is no data available for absorption coefficients, α, for polycrystalline mercuric iodide thin films, data was taken from single crystal films, shown below [39]:

Table 5.2: Absorption Co-efficients Used in Simulation

Wavelength λ (nm)	Absorption coefficient, α (cm^{-1})
400	3.2e5
410	2.97e5
420	2.55e5
430	2.15e5
440	1.9e5
450	1.55e5
460	1.5e5
470	1.3e5
480	1.25e5
490	1.2e5
500	1.1e5
510	1e5
520	9e4
530	7e4

Table 5.2(Continued)

540	6.5e4
550	6e4
560	2e4
570	700
580	300
590	70
600	11
610	5
620	3.5
630	0.8

5.2 Spectral Response and I-V Measurements

For the optical measurements on Mercuric Iodide thin films, an Oriel ¼ m monochromator was used .A focusing lens was used to concentrate the incident light onto a single spot of the thin film. A LabView™ data-logging program was used to record the measurements. The incident flux is obtained from the standard reference Si-Solar cell. Bias orientation is with respect to polarity of the illuminated electrode, i.e., the front contact. Dark I-V, Light I-V and Spectral response at negative bias of 50 V were measured for each sample. These measurements were then correlated with the simulations to better understand the photoexcited charge carrier kinetics under bias.

The layout of current Mercuric-iodide thin film samples is shown in figure 5.1.

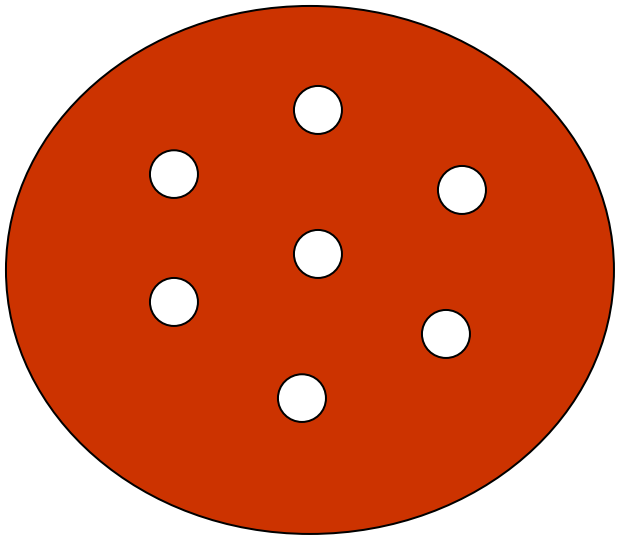

Figure 5.1: Layout of Current Typical Polycrystalline Mercuric Iodide Thin Film Samples

The film is 2.5 cm in diameter. Palladium (Pd) contacts are then sputtered onto the film through a mask. The contact size is 0.1 cm^2 . The seven contact points, shown in Figure 5.1 are defined by the Pd electrodes. The long term objective of this project is to grow films for large surface area medical imaging applications. For such applications, it is very important that photoresponse at every point on the film be uniform as the output from a number of points on the film is collated to form the final image [38].

5.3 Simulation of Spectral Response

Each contact point on the thin film is simulated in MEDICI^{TM} .The grid implemented in simulation is shown in figure 5.2.

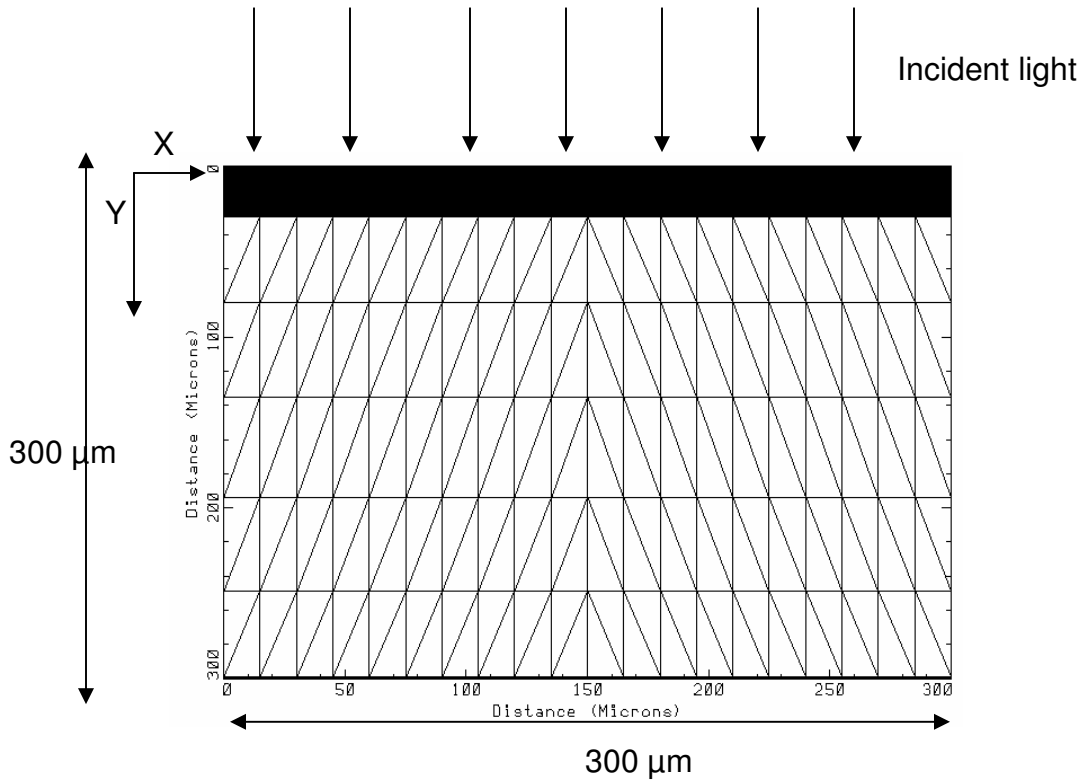

Figure 5.2: MEDICI Grid for the Mercuric-Iodide Thin Film

The optical and other data required for the HgI_2 in the simulation are shown in tables 5.1 and 5.2. The description of the light source and the ray-tracing parameters to simulate the spectral response are given in the PHOTOGEN statement shown in the Appendix. The solar light spectrum is approximated by the black body radiation spectrum at 5800 K. The number of sampled wavelengths, WL, is set to 25. Simulation is done for 25 wavelengths from 400 nm to 640 nm. Each wavelength has its monochrome component of light intensity calculated internally by MEDICI. The solution files obtained after the simulation is finished are called log files. The log files created after the simulation of spectral response is finished contain the following data:

1. Transmittance
2. Reflectance

3. Terminal currents
4. Number of photogenerated carriers
5. Incident, absorbed flux
6. Spectral response

5.4 Simulation of Light I-V Characteristics

Light I-V simulations are done at a single wavelength. The flux or intensity and wavelength at which light I-V characteristics to be obtained have to be mentioned in the code. I-V characteristics can be obtained for broad range of voltages. In this part of the effort, I-V characteristics were done from -50 V to + 50 V.

Part of the incident light is absorbed, some of it is transmitted and the rest is reflected. The absorption profile depends on the absorption coefficient α. The reflectance for each λ is calculated from the refractive index (n) and k, extinction coefficient. A bandgap of 2.13 eV corresponds to a cutoff wavelength, λ of 582.5 nm. The wavelengths beyond 582.5 nm are weakly absorbed, therefore they just pass through the material without generating many electron-hole pairs in the material.

The reflectance is calculated from the following equation:

$$R= ((n_1-n_2)^2 + k^2) / ((n_1+ n_2)^2 + k^2) \quad (5.1)$$

$$k = (\alpha * \lambda) / (4 * \pi), \quad (5.2)$$

Where k is the extinction co-efficient, n_1 and n_2 are the refractive indices of the two mediums.

The Calculated Reflectance data is given in the following table 5.3:

Table 5.3: Calculated Reflectance from Simulation

Wavelength λ (nm)	Reflectance(%)
400	27.64
410	27.17
420	26.15
430	25.24
440	24.74
450	24.06
460	24.02
470	23.69
480	23.64
490	23.6
500	23.45
510	23.31
520	23.18
530	22.9
540	22.85
550	22.81
560	22.48
570	22.44
580	22.44
590	22.44
600	22.44

Table 5.3(Continued)

610	22.44
620	22.44
630	22.44
640	22.44

The behavior of polycrystalline mercuric iodide thin films using MEDICI™ has been simulated, and the results have been interpreted. This chapter documents the simulated results of spectral response under -50 V bias and Light I-V characteristics. The objective of the simulation is to determine the mobilites, bulk lifetimes and surface recombination velocities of electrons and holes that would match the measured results with simulated results.

Typical spectral responses obtained from measurement of current mercuric iodide thin films are shown in figure 5.3.

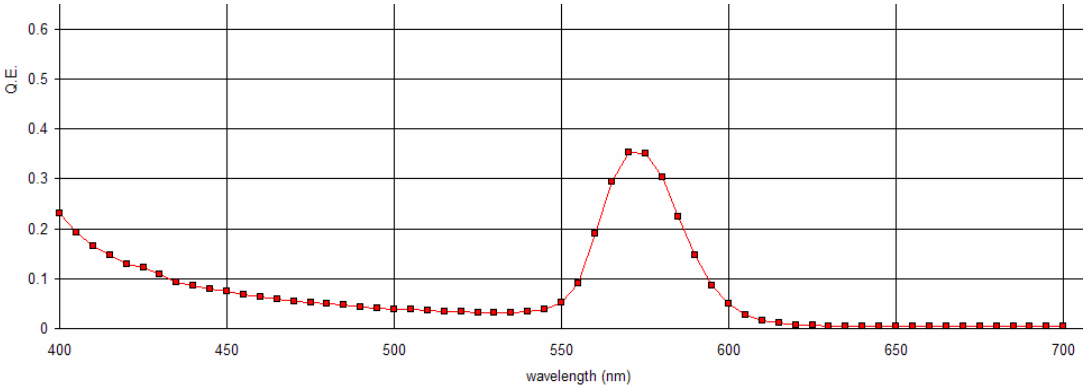

(a)

Figure 5.3: Typical Measured Spectral Response

(a) Very high Blue Response (b) Zero Blue Response (c) High Blue Response

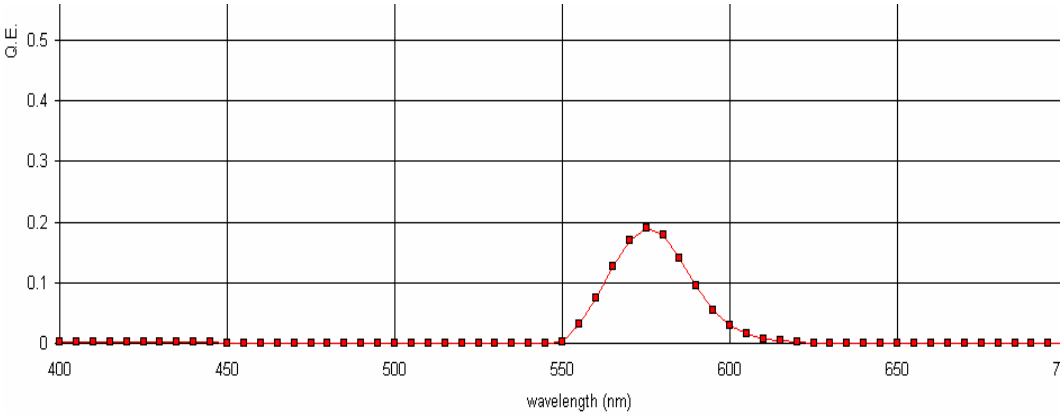

(b)

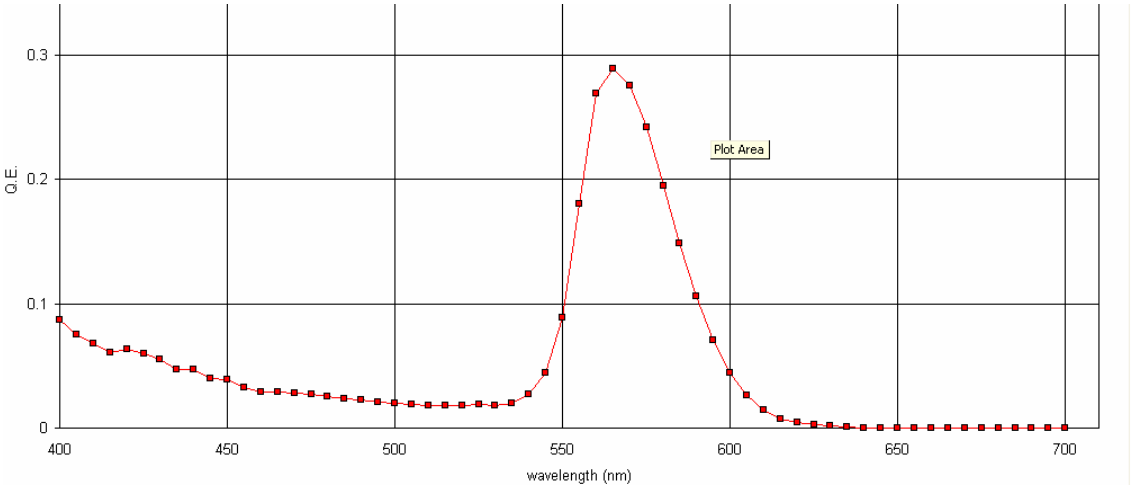

(c)

Figure 5.3(Continued)

The key observations that can be made from the above spectral response plots are:

1. The peak of response lies at 570 mm
2. For some of the plots, the SR drops from 400 nm to 540 nm and then reaches the peak at 570 nm. For some other plots, the SR is almost zero and flat from 400 nm to 540 nm and then reaches the peak at 570 nm. The blue SR was not obvious and was the most important, challenging part of the curve to be fitted.

In 1983, Levi et al [17] pointed out that whenever carriers are generated sufficiently close to the surface, surface recombination of charge carriers sets in, in addition to bulk trapping. In HgI_2 thin films the wavelengths (400-550) nm are very strongly absorbed due to the large absorption coefficient. The carriers are generated close to the surface, therefore the shape of the spectral response curve for this set of λ's is sensitive to surface as well as bulk recombination. Traditionally the influence of the surface on excess charge carrier kinetics is taken into account by boundary conditions, and surface recombination is described by the surface recombination velocity.

When all the electron hole pairs that are created due to absorption of photons are collected, we get unity Internal Quantum-Efficiency (IQE). The difference between internal and external QE (EQE), generally referred to as QE, in this case, is due to the optical losses, which are transmission and reflectance losses. Reflectance loss is dominant for strongly absorbed light. Both the losses affect the response for weakly absorbed light.

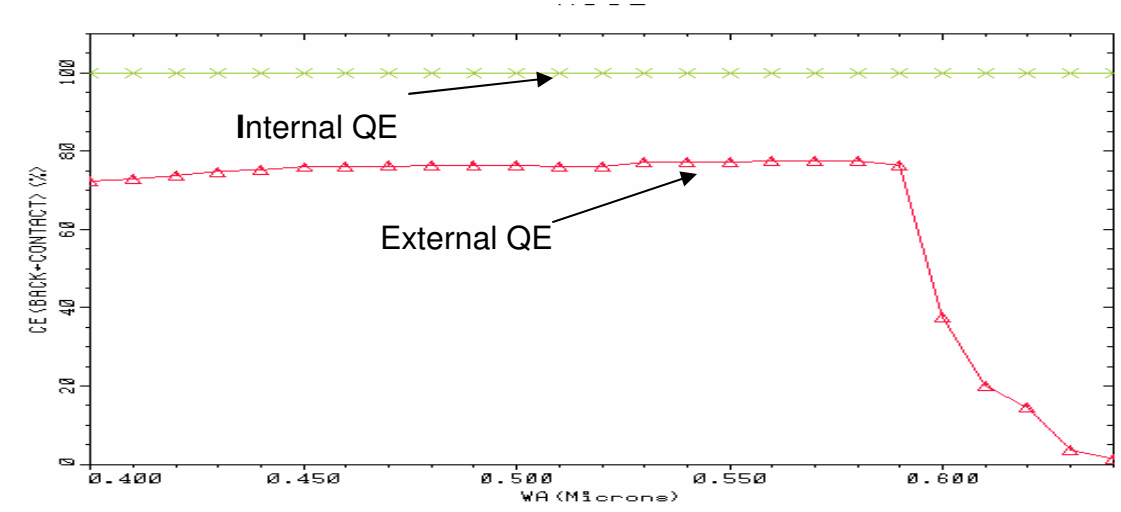

Figure 5.4: Typical Spectral Response Plot from Simulation to Illustrate IQE, QE

From figure 5.4, for wavelengths (400-590) nm, reflection loss is very clear from the external and internal spectral responses. For the wavelengths (590-640) nm, transmission and reflection losses make the external spectral response drop down significantly.

Carrier recombination is the only electrical loss mechanism in our devices which makes internal QE less than unity. As long as an appreciable electric field is present, the excess charge carriers are separated by the field and cannot participate in bulk or in surface recombination. SRH Bulk and Surface recombination models, the most probable recombination mechanisms that can occur in mercuric iodide thin films, are used in the simulations. The effect of bulk and surface recombinations on the spectral response has to be clearly understood before the curve-fitting of spectral response. The surface recombination velocities of electrons and holes for the back contact did not affect the spectral response. Hence in the following results the documented surface recombination velocities are understood as that for the front contact. The measured spectral responses are external QE, hence in the following results, measured and simulated spectral responses are understood as external QE's.

5.5 Mismatch of Blue Spectral Response

The simulated spectral response with parameters from tables 5.4 and 5.5 matched a part of the measured spectral response i.e., for wavelengths (570-640) nm but failed to match the measured spectral response for wavelengths (400-570) nm for devices with blue response. The simulated and measured spectral response plots are shown in figure 5.5.

Table 5.4: Surface Recombination Parameters for Mismatched Blue Response

Carrier	Surface recombination velocity (cm s^{-1})
Electron	1e10
Hole	1e10

Table 5.5: Bulk Recombination Parameters for Mismatched Blue Response

Carrier	Mobility(cm^2 / V. s)	Lifetime(sec)
Electron	3.5	4e-7
Hole	0.1	6e-8

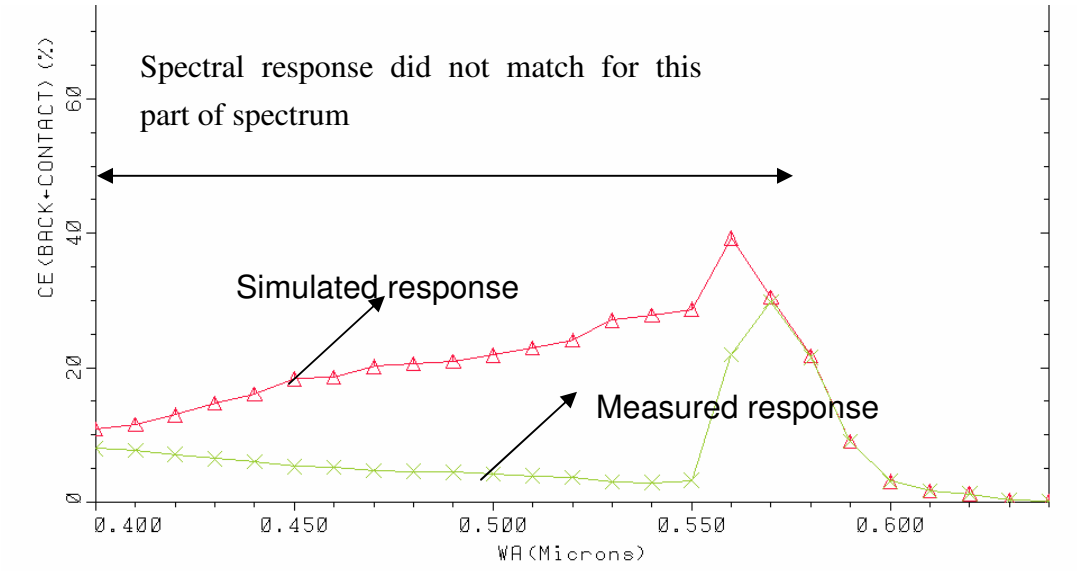

Figure 5.5: Mismatch of Blue Spectral Response

Though very high values of 1e10 cm s^{-1} for surface recombination velocities which are expected to make the carriers generated on the surface recombine were used, the simulated blue response did not go down as was required by the measured response. Surface recombination velocities less than 1e10 cm s^{-1} make the blue response still higher

as shown in figure 5.6. The mismatch of measured and simulated blue response is clear from figure 5.5.

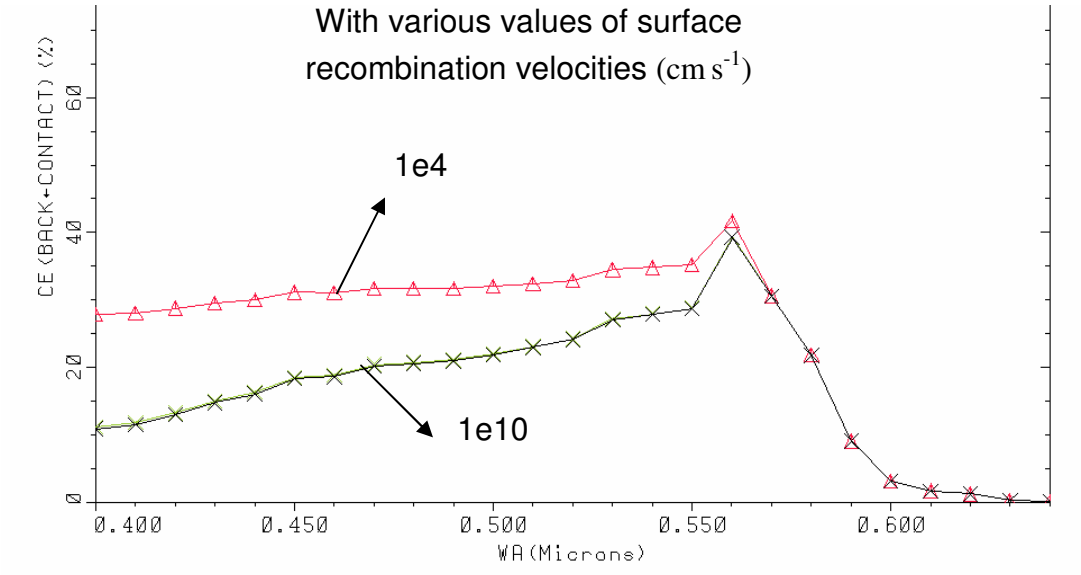

Figure 5.6: Simulated Spectral Response Vs Surface Recombination Velocity

The values of μτ in table 5.5 were large enough to make the blue response higher, but were needed to make the long wavelength region match the measured response. The overall spectral response was sensitive to the bulk recombination. Higher (smaller) values of μτ increases (decreases) the overall Spectral response, the plots of which are shown in figure 5.7.

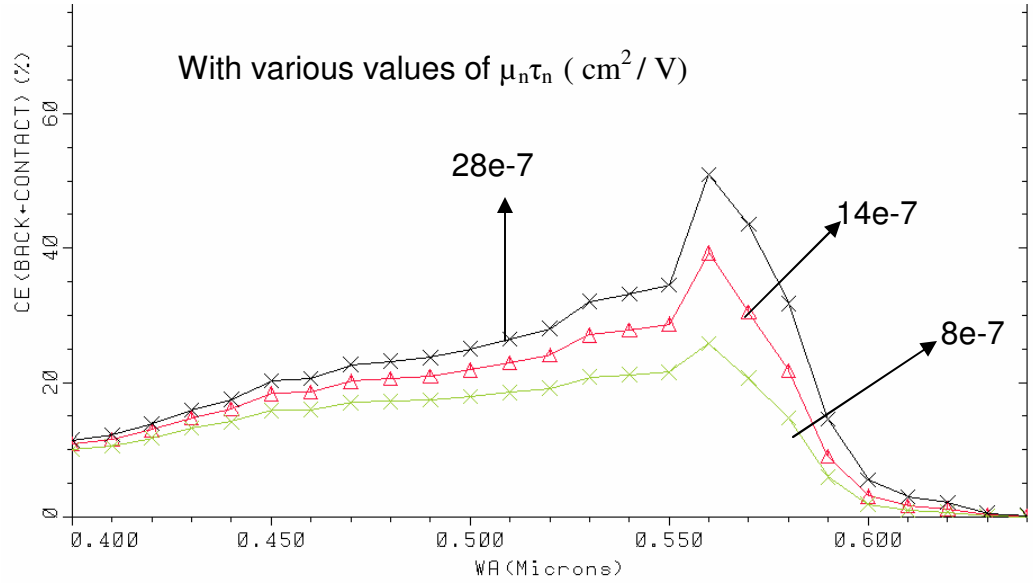

Figure 5.7: Simulated Spectral Response as a Function of $\mu_n\tau_n$

From the above figures 5.5, 5.6 and 5.7, it can be concluded that the mobilites of 3 for electron and 0.1 for hole, bulk lifetime of 4e-7 s for electron and 6e-8 s for hole are needed to make the long wavelength region match the measured response. The simulated blue response did not match the measured blue response for any combinations of bulk and surface recombination parameters.

5.6 Match of Blue Spectral Response

The simulated spectral response with parameters from tables 5.6 and 5.7 matched a part of the measured spectral response i.e., for wavelengths (400-570) nm but failed to match the measured spectral response for wavelengths (570-640) nm. The simulated and measured spectral response plots are shown in figure 5.8.

Table 5.6: Surface Recombination Parameters for Matched Blue Response

Carrier	Surface recombination velocity (cm s^{-1})
Electron	1e2
Hole	1e2

Table 5.7: Bulk Recombination Parameters for Matched Blue Response

Carrier	Mobility(cm^2 / V. s)	Lifetime(sec)
Electron	1	5e-10
Hole	0.01	5e-10

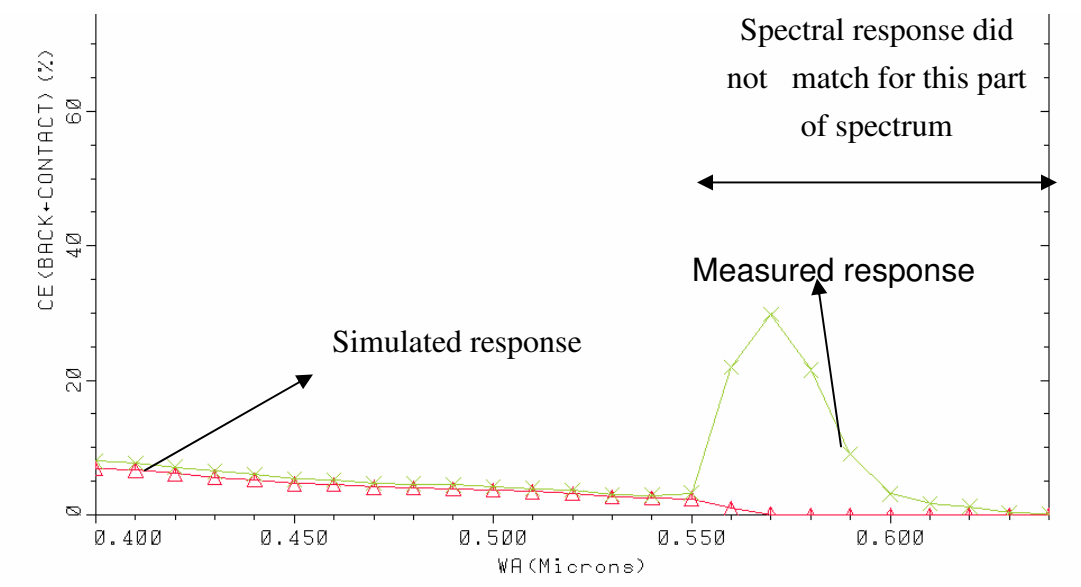

Figure 5.8: Match of Blue Spectral Response

With the parameters from tables 5.6 and 5.7, when the surface recombination velocity for holes was increased (reduced), this increased (reduced) the simulated blue response. From figure 5.9, for a given set of μτ, i.e., for the set of μτ in table 5.7, a surface recombination velocity of 1e4 cm s^{-1} for holes increased the blue response, whereas values of 10 and 1 cm s^{-1} reduced the blue response. Therefore it can be concluded that it is the competition between the two opposing mechanisms, surface recombination and bulk recombination that determines the blue response. The surface recombination mechanism produces an effective surface field proportional to surface recombination velocity of holes that pulls the holes that are generated away from the

surface towards the surface, thereby helping the holes escape from bulk recombination with electrons. Photogenerated holes are lost through bulk recombination with electrons when bulk recombination dominates lower surface fields.

With the parameters from tables 5.6 and 5.7, when the surface recombination velocity for electrons was increased, the simulated blue response was reduced. As seen in figure 5.10, for a given value of μτ, such as that in table 5.7, a higher surface recombination velocity of 1e5 cm s^{-1} for electrons reduced the blue response.

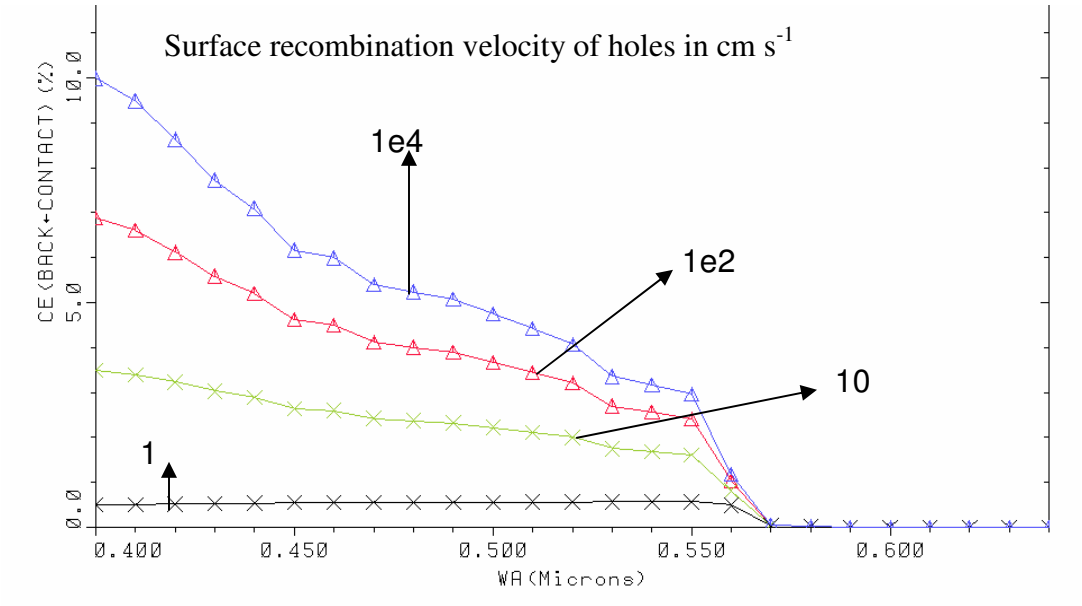

Figure 5.9: Blue Response as a Function of Surface Recombination Velocity of Holes From 1 to 1e4 cms^{-1}

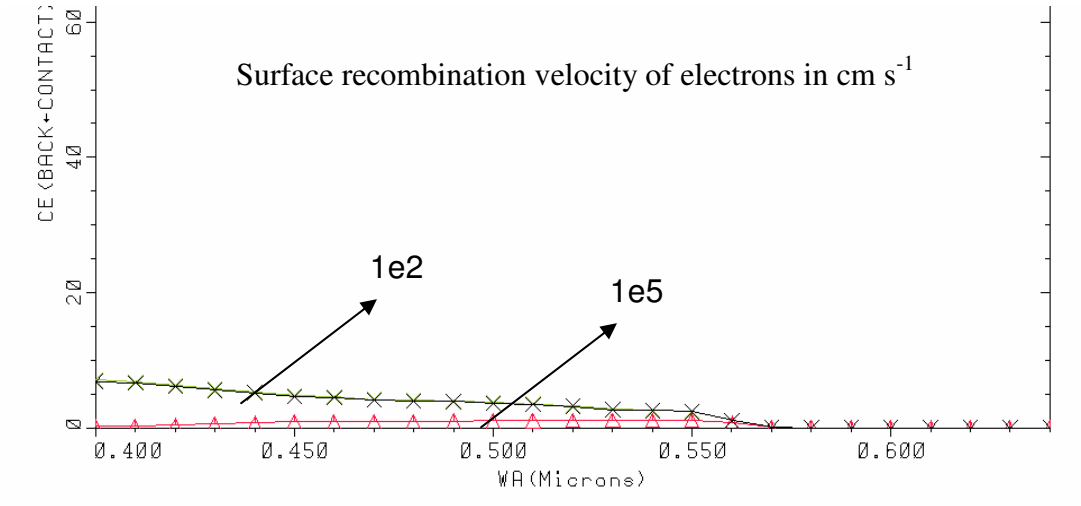

Figure 5.10: Blue Response as a Function of Surface Recombination Velocity of Electrons of 1e2 and 1e5 cms^{-1}

From figures 5.8, 5.9 and 5.10, the simulated long wavelength response did not match the measured response. The values of μτ from table 5.7 were needed to make the blue response match the measured response, but were too small to match the long wavelength region response.

From the two sets of parameters in the above sections 5.5 & 5.6 i.e., from tables 5.4, 5.5 & tables 5.6, 5.7, one that matches the measured long wavelength response figure 5.5 and one that matches the measured blue response figure 5.8 respectively, we can conclude that there have to be two sets of bulk recombination parameters to get complete match of measured and simulated spectral responses. There can't be two sets of bulk recombination parameters for a single homogeneous region of 300μm.

5.7 Match of Complete-Spectral Response

The other possibility to two different sets of bulk recombination parameters is to have 2 different regions, and have different sets of mobilities and bulk lifetimes for each region.

The next step was to identify the widths of these two different regions. By a trial and error method, the simulated response matched the complete measured response of figure 5.11, when the first region of 0.5 µm width was chosen. Hence, the HgI_2 thickness of 300 µm is divided into two regions. The first region is 0.5 µm thick from the surface of SnO_2, and the remainder is 299.5 µm thick. The response in the first region is determined by the competition between the surface and bulk recombination. The response in the second region is bulk recombination dominated. The parameters determined from simulation for both the first and second regions that matched the complete measured spectral response are given in tables 5.8, 5.9 and 5.10.

Table 5.8: Surface Recombination Parameters for Complete Match of SR

Carrier	Surface recombination velocity (cm s^{-1})
Electron	1e2
Hole	1e2

Table 5.9: Bulk Recombination Parameters for the First Region (0-0.5) µm

Carrier	Mobility(cm^2 / V. s)	Lifetime(sec)
Electron	1	5e-10
Hole	0.01	5e-10

Table 5.10: Bulk Recombination Parameters for the Second Region (0.5-300) µm

Carrier	Mobility(cm^2 / V. s)	Lifetime(sec)
Electron	3.5	4e-7
Hole	0.1	6e-8

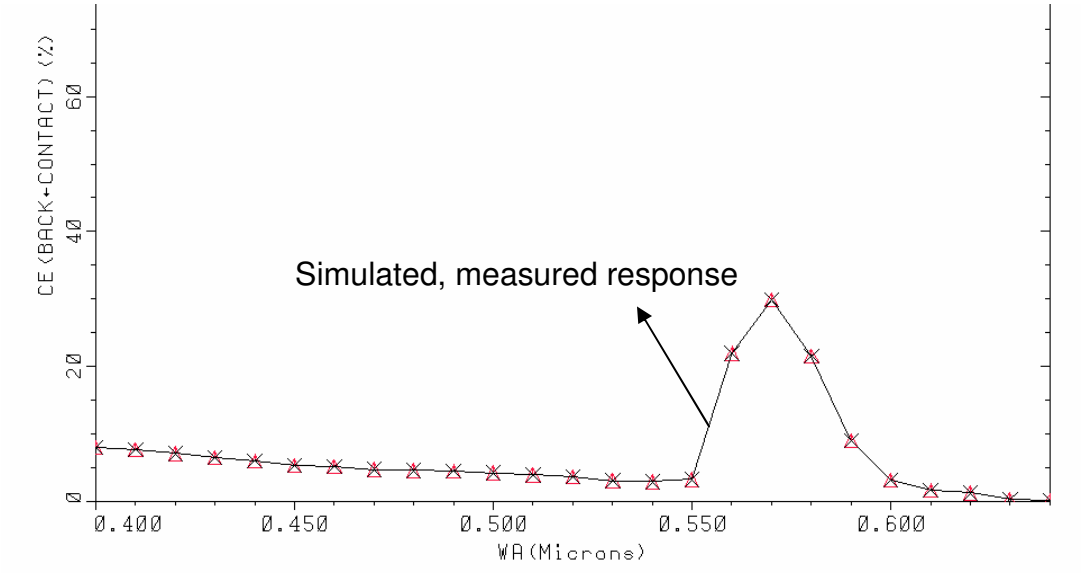

Figure 5.11: Complete Match of Spectral Response

The spectral response plots with the set of parameters given in tables 5.8, 5.9 and 5.10 for various widths of the first region are shown in figure 5.12.

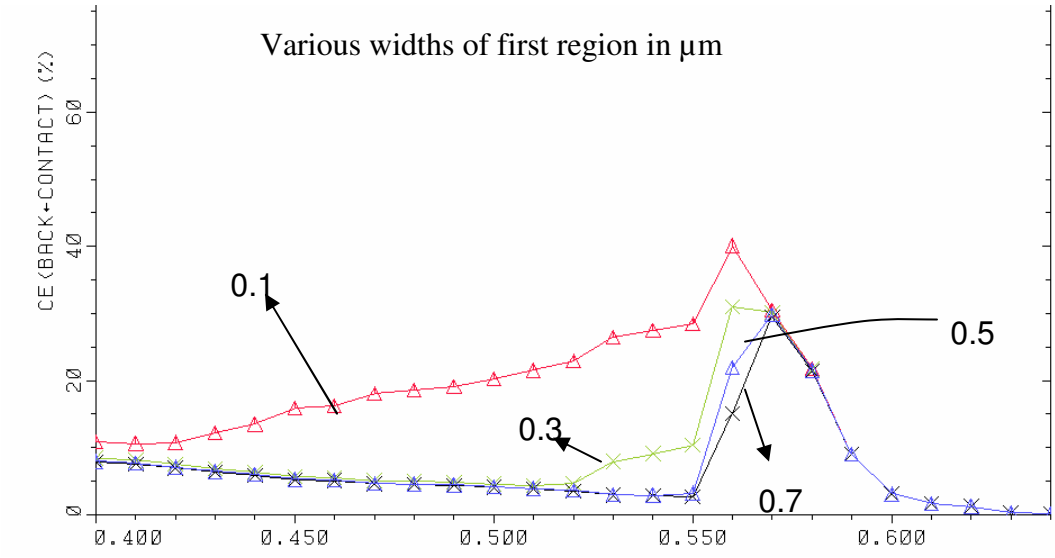

Figure 5.12: Spectral Response Plots Vs Widths of the First Region

Figure 5.12 shows the simulated SRs for various widths of the first region, 0.1µm, 0.3 µm, 0.5 µm and 0.7 µm. It is evident from figure 5.12 that the first region of 0.5 µm in the two-region model exactly matches the complete measured response.

In some of the measured spectral responses from figure 5.3 (b), the blue spectral response was flat and zero. Simulated responses matched those measured responses when surface recombination velocities of electrons and holes were varied in the two-region model.

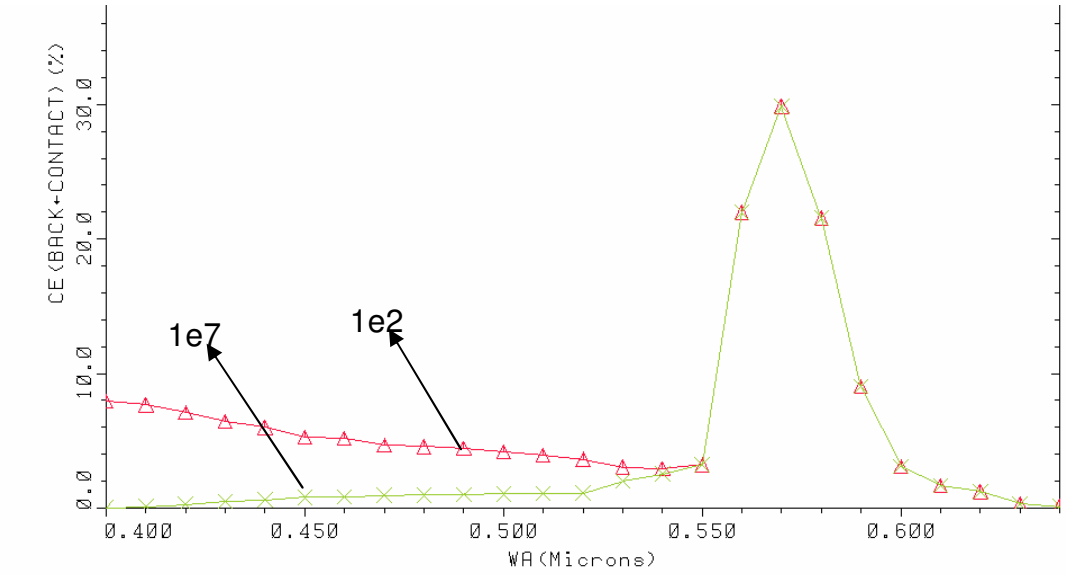

Figure 5.13: QE Vs λ for Electron Surface Recombination Velocity of 1e7 and 1e2 Cms^{-1}

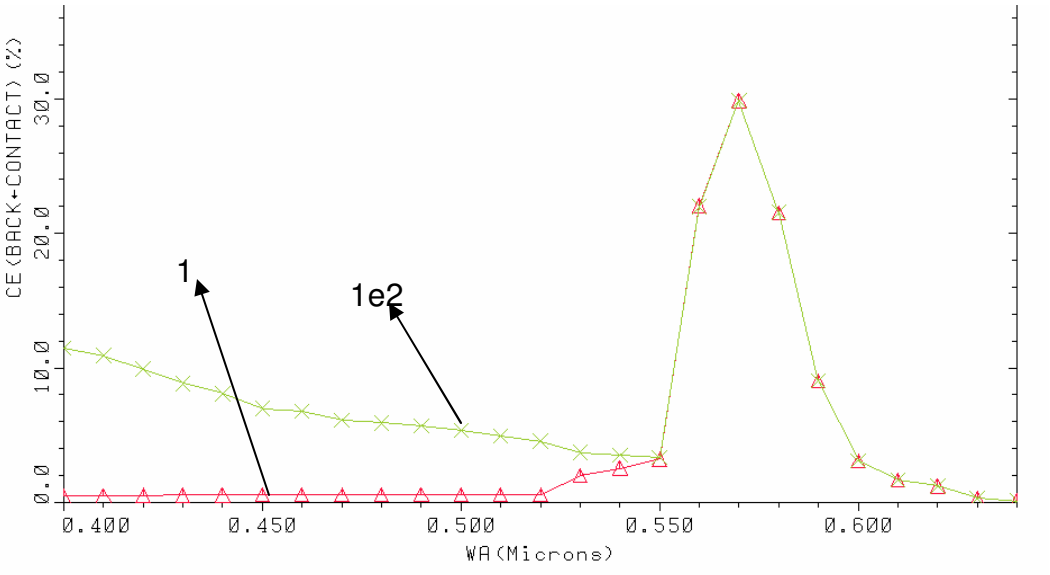

Figure 5.14: QE Vs λ for Hole Surface Recombination Velocity of 1 and 1e2 Cms^{-1}

From figure 5.13 a higher surface recombination velocity for electrons of 1e7 cm s^{-1} makes the blue response flat and almost zero. From figure 5.14 a lower surface recombination velocity for holes of 1 cm s^{-1} makes the blue response flat and almost zero. The physics behind these blue responses was explained earlier in section 5.6.

Hence, the two-region model developed in MEDICI^{TM} was able to explain most of the measured spectral responses of current HgI_2 thin films. However, there were a few drawbacks of this model. The drawbacks are explained in the following section.

5.8 Drawbacks of the Two-region Model

There were two main drawbacks of the two region model.

1. Incomplete match in blue spectral response.
2. Incomplete match of light I-V characteristics.

5.8.1 Incomplete Match in Blue Spectral Response

Some of the measured blue spectral responses of mercuric iodide thin films were very high as shown in figure 5.3 (a). Simulated spectral responses with the two region model failed to match such higher blue responses. Though the highest reasonable values of surface recombination velocity for holes of 1e6 cm s^{-1} and the lowest reasonable surface recombination velocity for electrons of 0.1 cm s^{-1} were picked, the simulated blue response did increase as was expected, but was not high enough to match the measured response of figure 5.3 (a). The plots are shown in figure 5.15.

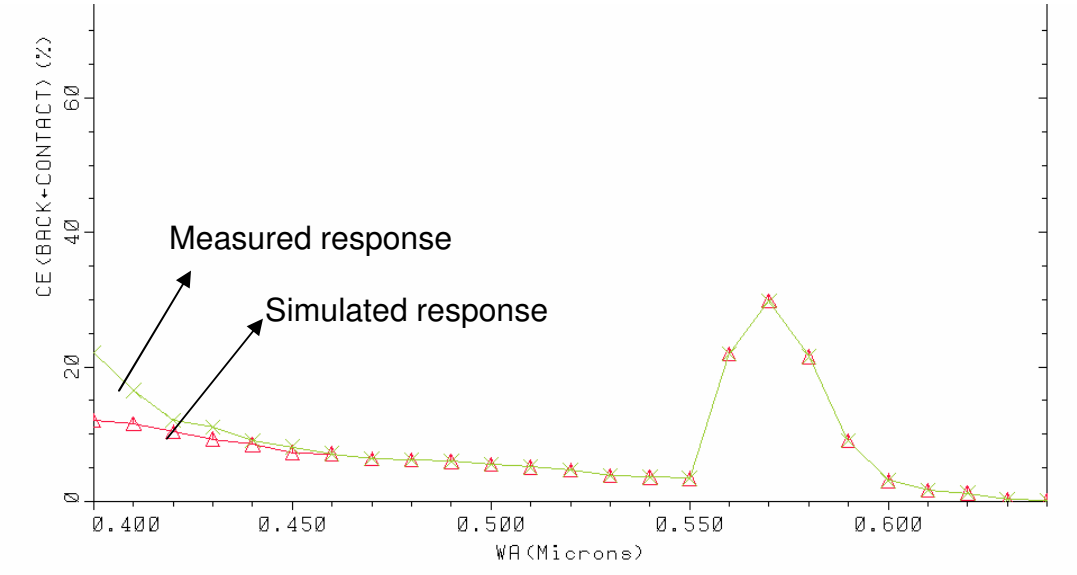

Figure 5.15: QE Plots for Simulation Vs Measurement Showing Limitations in Blue Spectral Response

As there was considerable instability in the measured photocurrents, the measured spectral response may not be accurate, or the model developed in this effort might be incomplete to explain such higher blue responses.

5.8.2 Incomplete Match of Light I-V Characteristics

The peak of the measured spectral responses for most of the current Mercuric Iodide thin film samples is at 570 nm. When the two region model was used to simulate light I-V characteristics at 570 nm, the simulated light I-V curve did not match completely the measured light I-V characteristics. The mismatches observed in the measured and simulated curves are shown in figure 5.16. The incident photon flux levels for 400,500& 570 nm are given in table 5.11. There was considerable saturation of photocurrent for positive applied biases in measured light I-V characteristics. Simulations failed to obtain such saturation in photocurrents.

Table 5.11: Wavelengths Vs Incident Photon Flux Levels

Wavelength(nm)	Incident Photon Flux(photons/ sec)
400	2.76e12
500	2.39e13
570	4.45e13

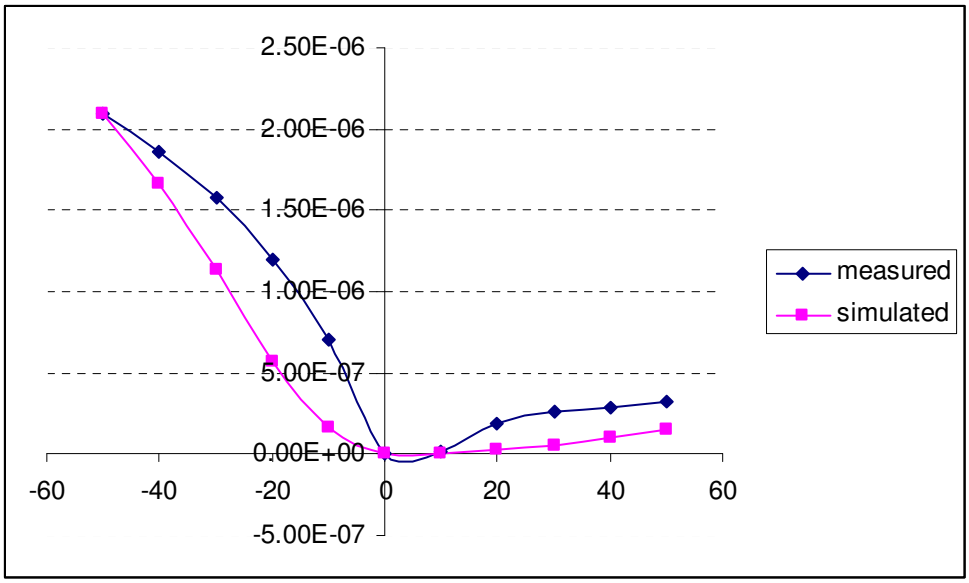

Figure 5.16: Light I-V Characteristics at 570 nm

The simulated light I-V characteristics in figure 5.16 were obtained with input parameters from tables 5.8, 5.9 & 5.10. From figures 5.13 & 5.14, response at 570 nm is independent of the surface recombination parameters. Hence, the simulated light I-V characteristics in figure 5.16 remain unaltered when surface recombination velocities were varied. However from figures 5.13 & 5.14, blue response was seen as a function of surface recombination velocities. Simulated light I-V characteristics at 400 and 500 nm as a function of surface recombination velocities are shown in figures 5.17, 5.18, 5.19 & 5.20.

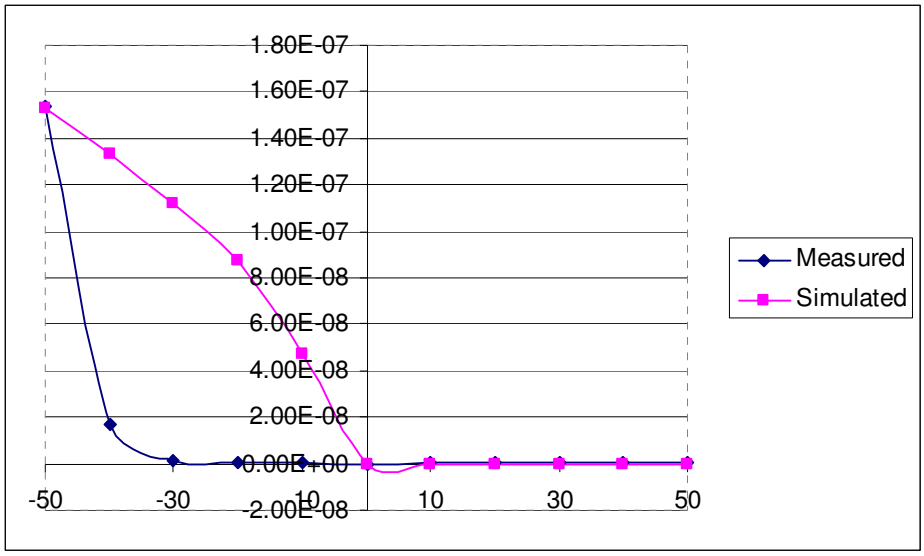

Figure 5.17: Light I-V Characteristics at 400 nm for Non-Zero Blue SR

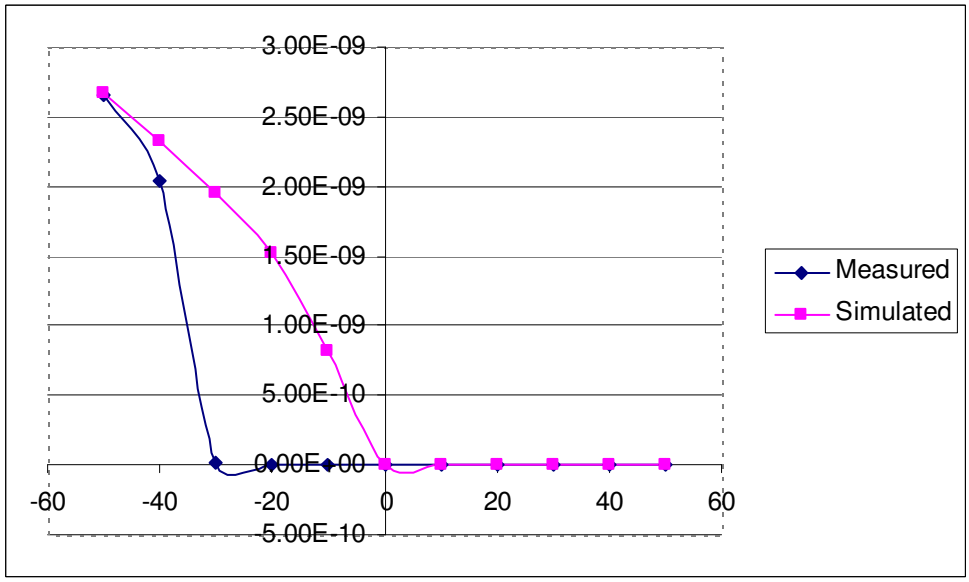

Figure 5.18: Light I-V Characteristics at 400 nm for Zero Blue SR

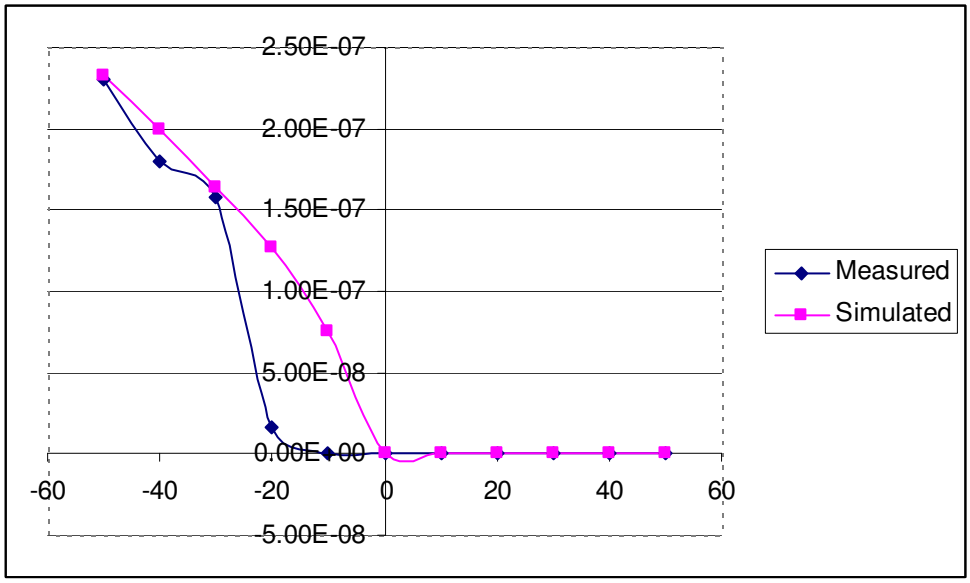

Figure 5.19: Light I-V Characteristics at 500 nm for Non-Zero Blue SR

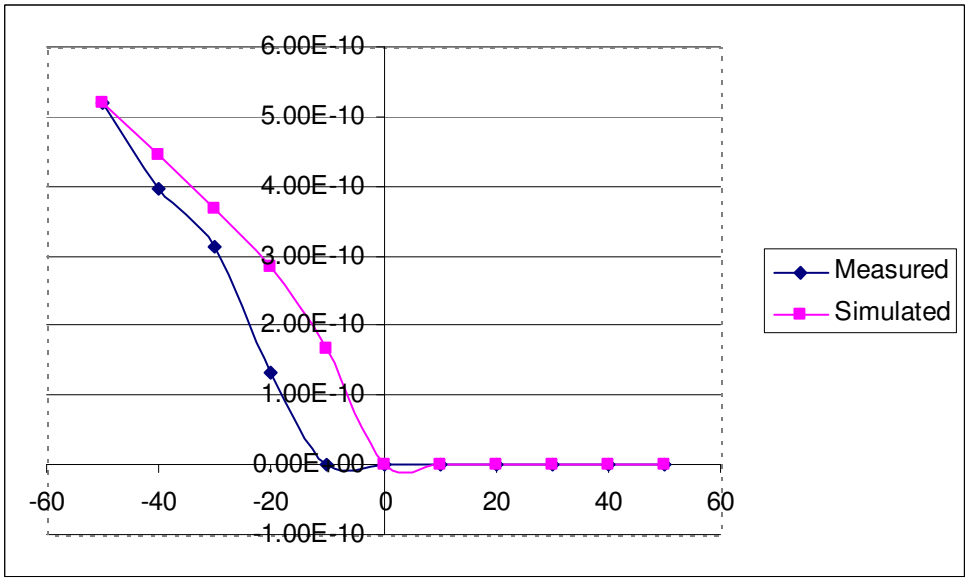

Figure 5.20: Light I-V Characteristics at 500 nm for Zero Blue SR

The simulated light I-V characteristics in figures 5.17, 5.18, 5.19 & 5.20 were obtained with input parameters from tables 5.8, 5.9& 5.10. Surface recombination velocity for holes of 1 cm/s was used to get zero blue SR, from figure 5.14. Simulated photocurrents for positive polarities in figures 5.17, 5.18, 5.19 & 5.20 were negligible

and experimentally were unmeasurable. There was no complete match of measured and simulated light I-V characteristics for negative polarities in these figures. The model developed in this part of the work might be incomplete as measured and simulated light I-V characteristics did not match completely though measured and simulated spectral responses matched. As there was considerable instability in measured photocurrents especially in the blue spectral region, the measured light I-V characteristics may not be accurate.

CHAPTER 6

CONCLUSIONS

6.1 Conclusions

This research has used the capabilities of computer simulation to perform the modeling of QE and I-V characteristics of Mercuric Iodide thin films with the DC device modeling tool, MEDICI^{TM}. Several polycrystalline HgI_2 thin films were studied as part of this effort. Mobilities, lifetimes for carriers are known for single crystals and can be obtained from the literature. In the case of polycrystalline films, these parameters are strongly dependent on the processing conditions and thus are yet unknown. By comparing the simulated and measured spectral responses, we have obtained these parameters. The values for input parameters used in simulation were chosen from the literature, theory and reasonable estimates. Comprehensive studies were performed to investigate the sensitivity of Spectral Response and light I-V characteristics to each input parameter. Recombination within the bulk and at the surfaces have been investigated in this thesis.

Blue spectral response was of main concern in this part of the research. A Single, homogeneous region with all possible combinations of carrier mobilities, surface and bulk recombination parameters did not match completely the measured spectral response. To have complete match of measured and simulated spectral responses, simulations suggested a two region model for Mercuric Iodide thin films of 300 μm thickness. The

first region extends 0.5 μm from SnO_2, and the second region is 299.5 μm thick. Each region has different sets of mobilities and bulk lifetimes for both carriers. For complete match of some of the measured spectral responses, the determined values for the first region are bulk lifetimes of 5e-10 s for both carriers, mobility of 1 cm^2 / V-s for electrons and 0.01 cm^2 / V-s for holes. For the second region, the values are bulk lifetime of 4e-7s for electrons and 6e-8 s for holes, mobility of 3 cm^2 / V-s for electrons and 0.1 cm^2 / V-s for holes. There were two extremes of measured blue response, a considerable blue response (figure 5.3 (c)) and a zero blue response (figure 5.3 (b)) .The two-region model explained both these kinds of blue responses. The blue response was found to be a function of surface recombination velocities of electrons and holes, for a given set of mobilities and bulk lifetimes of the carriers. A Surface recombination velocity at the front contact of 100 cm s^{-1} for both electrons and holes was determined from simulation to be needed for considerable blue spectral response. A Surface recombination velocity of 1 cm s^{-1} for holes or 1e7 cm s^{-1} for electrons was determined from simulation to obtain zero blue spectral response.

Simulations failed to match some of the very high measured blue responses as illustrated in section 5.8.Simulated light I-V characteristics did not match completely the measured ones. The model developed to the level attained here may require additional features for Mercuric Iodide thin films. More careful measurement of I-V curves is also warranted to account for time variations.

6.2 Future Work

This research serves as a major step towards device modeling of spectral response and I-V characteristics of Mercuric Iodide thin films. We have been successful in

determining a set of mobilities, lifetimes, and surface recombination velocities of carriers that can match some of the measured spectral responses of current Mercuric Iodide thin films.

As there is instability in the photoresponse, the following suggestions are made to improve the integrity of the experimental data.

Spectral response can be done as a function of the time elapsed between two incident wavelengths during measurement. They can also be done as function of incident photon flux levels. These measurements might help gain insights into the shortcomings observed in simulation.

If better fit to experiment is not attained once the experimental data is improved, then a more complex model of the material will be needed for simulation.

REFERENCES

1. www.public.asu.edu/~ntao1/ECE352/ECE04-11.ppt.

2. W.Shockley,Phys.Rev,Vol 56,pp.317-325,Aug 1935.

3. R.H.Kingston(ed),"Semiconductor surface physics", University of Pennsylvania press, 1956.

4. M.Ito,O.Wada IEEE Journal of Quantum electron Vol 22,pp. 1073,1986.

5. S.M.Ryvkin,photoelectric effects in semiconductors,consultants Bureau, New York 1964.

6. Semiconductors for room temperature nuclear detector applications, Vol43.

7. D.V.Chepur, Nauk, Povidomlenija university, 1(1956) 30.

8. W.R.Wilig.Nucl.Instruments, methods in phys.Res. 96 (1971)615.

9. P.F.Berry and G.R.Voots,"on-site verification of alloy materials with a new field-portable XRF analyzer based on a high resolution HGI2 semiconductor x-ray detector" in the proceedings of the 12th world conference on Non-Destructive testing,Amsterdam,The Netherlands, April 1989,pp 737-742.

10. Characterization of single-crystal mercuric iodide, Nuclear Instruments and Methods in Physics Research Section A: Accelerators, Spectrometers, Detectors and Associated Equipment, Volume 517, Issues 1-3, 21 January 2004, Pages 226-229 D. Alexiev, N. Dytlewski, M. I. Reinhard.

11. Current instability in mercuric iodide devices, Solid-State Electronics, Volume 44, Issue 1, January 2000, Pages 29-35 J. P. Ponpon, R. Stuck and M. Amann.

12. M.Schieber, W.F.Schnepple and L.van Den Berg, J.crystal growth 33(1976)125.

13. D.S. McGregor et al.,"Room temperature semiconductor radiation detectors".

14. M. Piechotka, "Mercuric Iodide for room temperature radiation detectors. Synthesis, purification, crystal growth and defect formation", Materials Science and Engineering 18 I-98, Elsevier Science S.A., 1997.

15. Characterization of carrier generation and transport mechanisms in single-crystal and thin-film HgI_2 ,U. Khadilkar, R. Mamazzaa, C. S. Ferekides, D. L. Morel R. DeVito, J. Sandoval and L. van den Berg Thin Solid Films Vol 427, Issues 1-2, 3 March 2003, Pages 381-385.

16. www.ece.umd.edu/~davis/chapter22.pdf.

17. A.Levi, M.Schieber, Z.Burshtein, "Carrier surface recombination in HgI_2 photon detectors," J.Appl.Phys., vol 54, pp 2472-2476, 1983.

18. "Near single-crystal electrical properties of polycrystalline HgI_2 produced by physical vapor deposition". A. Zuck, M. Schieber, O. Khakhan and Z. Burshtein. Proc. of the IEEE Nuclear Science Symposium Conference I, 505 (2002).

19. http://oregonstate.edu/dept/nchem/textbook/chapter17.pdf.

20. http://userpages.umbc.edu/~rczebo1/research/ch1.pdf.

21. A.Rose,Phys.,Rev.,97 (1955) 1538.

22. M.A.Lampert,Phys.,Rev.,103 (1956) 1648.

23. N.El-Kadry,A.Ashour,S.A.Mahmoud, "Structural dependence of D.C.electrical properties of physically deposited CdTe thin films", Thin Solid Films 269 (1995) 112-116.

24. J. S. Blakemore, Semiconductor Statistics, International Series of Monographs on Semiconductors, Vol. 3, Pergamon Press, Oxford (1962).

25. D. K. Schroder, Semiconductor Material and Device Characterization, 2nd edition: John Wiley and Sons, (1998).

26. W. Shockley and W. T. Read, "Statistics of the Recombinations of Holes and Electrons" Phys. Rev., **87** , pp. 835-842, (1952).

27. R. N. Hall, "Electron-Hole Recombination in Germanium" *Phys. Rev.*, **87,** pp. 387,(1952).

28. R. Hacker and A. Hangleiter, “Intrinsic upper limits of the carrier lifetime in silicon” J.Applied. Phys., **75** (11), pp. 7570-7572, (1994).

29. H. Schlangenotto, H. Maeder, and W. Gerlach, “Temperature Dependence of the radiative Recombination Coefficient in Silicon” Physica Status Solidi, **21a,** pp. 357-367, (1974).

30. Hangleiter and R.Hacker, “Enhancement of Band-to-Band Auger Recombination by electron-Hole Correlations” *Physical Review Letters*, **65** (2), pp. 215-218, (1990).

31. R. F. Pierret, Advanced Semiconductor Fundamentals, vol. VI: Addison-Wesley, (1989).

32. G. Aberle, S. W. Glunz, and W. Warta, “Impact of illumination level and oxide parameters on Shockley-Read-Hall recombination at the Si-SiO2 interface” Journal of Applied Physics. 71 (9), pp. 4422-4431, (1992).

33. E. Rimini, J. Haskell, and J. W. Mayer, Appl. Phys. Lett. 20, 237 (1972).

34. G. Masetti, M. Severi, and S. Solmi, IEEE Trans. Electron Devices ED-30, 764 (1983).

35. E. Yablonovitch, R. M. Swanson, W. D. Eades, and B. R. Weinberger, Appl. Phys.Lett. 48, 245 (1985).

36. T Otaredian, “The influence of the surface and oxide charge on the surface recombination process,” Solid-State Electron., vol. 36, pp.905–915, June 1993.

37. David S. L. Mui, L. A. Coldren,”Effects of surface recombination on carrier distributions and device characteristics “, Journal of Applied Physics, 78 pp 3208-3215(1995).

38. Unmesh Khadilkar,” Modeling and characterization of polycrystalline mercuric Iodide Radiation detectors”, Master’s Thesis, University of South Florida, 2003.

39. Yao, H, Johs, B, and James, R.B., 1994, “semiconductors for room temperature nuclear detector applications”, semiconductor and semimetals Vol43.

40. MEDICI 2-D Semiconductor device simulator ver 4.3, Avant Corp.,Palo Alto, CA 1999.

41. http://www.psu.edu/dept/AMPS/.

APPENDICES

Appendix I MEDICI ™

A sample program with comments is given below:

```
$ A program to simulate spectral response, plot the results

TITLE HgI2

$MESH

MESH

$ Mesh in X-direction

X.MESH        WIDTH=300 H1=15

$Mesh in Y-direction

$fine grid for (0-30) µm as most of the light is absorbed within 30 µm

Y.MESH        Y.MIN=0 Y.MAX=0.1 H1=0.001

Y.MESH        Y.MIN=0.1 Y.MAX=1 H1=0.003

Y.MESH        Y.MIN=1 Y.MAX=30 H1=0.5

$Fine grid as there is no absorption beyond 30 µm

Y.MESH        Y.MIN=30 Y.MAX=299 H1=50

$Fine grid to take into account of back-surface effects

Y.MESH        Y.MIN=299 Y.MAX=300 H1=0.1

$Definition of region as semiconductor

REGION        NAME=HGI21 Y.MIN=0 Y.MAX=0.5 SEMICOND

REGION        NAME=HGI22 Y.MIN=0.5 Y.MAX=300 SEMICOND

$ Location of electrodes

ELECTRODE  NAME=FRONT_CONTACT  TOP

ELECTRODE  NAME=BACK_CONTACT BOTTOM
```

Appendix I (Continued)

```
$Contact properties
CONTACT     NAME= FRONT_CONTACT  WORKFUNC=4.8
$Surface Recombination velocity for electron and hole
+SURF.REC VSURFN=1E-3 VSURFP=50
$Front contact is made 100% transparent
+TRANSELE
CONTACT     NAME= BACK_CONTACT WORKFUNC=4.8 SURF.REC
$Lower values were picked as there were convergence problems for value of zero
$Back contact is made 100% opaque
+VSURFN=1E-2 VSURFP=1E-2
$Semiconductor Material properties
MATERIAL   REGION= (HGI21, HGI22) PERMITTI=11 AFFINITY=4 EG300=2.13
+NC300=2.0E19 NV300=2.0E19
$Optical properties like Refractive Index, Absorption constants
MATERIAL   REGION= (HGI21, HGI22) WAVE.RE= (0.4, 0.7) INDEX.RE= (2.8, 2.8)
MATERIAL   REGION= (HGI21, HGI22) ABS.FILE=ab8 FIRST LAST
$Mobility values for different regions
MOBILITY    REGION=HGI21 MUN0=1 MUP0=0.01
MOBILITY    REGION=HGI22 MUN0=3.5 MUP0=0.1
$'Spatially and energetically uniform traps acting as Recombination centers, placed in
$mid-energy gap' lifetime for both carriers is given as input
TRAPS          TAUN=5e-10 TAUP=5E-10 COND=" (@Y>0.0) &(Y<0.5)"
```

Appendix I (Continued)

$'Spatially and energetically uniform traps acting as Recombination centers, placed in mid-energy gap' lifetime for both carriers is given as input

TRAPS TAUN=4e-7 TAUP=6E-8 COND=" (@Y>0.5) &(Y<300)"

$Fermi-dirac Statistics

MODELS FERMIDIR REGION= (HGI21, HGI22)

$Spectral Response at bias

SOLVE V (BACK_CONTACT) =0 ELEC= BACK_CONTACT

SOLVE V (FRONT_CONTACT) =-50 ELEC= FRONT_CONTACT

$Ray Tracing is done for wavelengths from 400 to 640 nm with a resolution of 10 nm, optical source is Black-Body radiation at 5800 K.

PHOTOGEN RAYTRACE BB.RADI BB.TEMP=5800 WAVE.ST=0.395 +WAVE.END=0.645 WAVE.NUM=25 X.ORG=150 Y.ORG=-5

$ Store the solution in a log file, which can be read later

+LOG OUT.FILE=SURF.IVL

$Solve at each wavelength

LOOP STEPS=25

SOLVE WAVE=1:1

L.END

$End of the Program

END

$To solve at one wavelength

SOLVE WAVE=1

Appendix I (Continued)

$solution is saved as TIF File and can be read to plot electric field, band-diagram, $electron and Hole concentration

SAVE OUT.FILE=5800-SOL-1 TIF

$code to read the solution files to plot several data in single graph

LOAD IN.FILE=5800-SOL-1 TIF

$1D plot of Electric Field along Y-direction

PLOT.1D E.FIELD X.ST=0 X.END=0 Y.ST=0 Y.END=300

$Code to plot Spectral Response from different LOG files in single graph

PLOT.1D IN.FILE=FILE_NAME1 X.AXIS=WA Y.AXIS=CE (BACK_CONTACT)

PLOT.1D IN.FILE=FILE_NAME2 X.AXIS=WA Y.AXIS=CE (BACK_CONTACT)

$To plot on the same graph

+UNCH

$Code to plot I-V from LOG File

PLOT.1D IN.FILE=FILE_NAME1 X.AXIS=V(FRONT_CONTACT) Y.AXIS=I(BACK_CONTACT)

$To plot positive and negative currents for both biases in one graph, absolute scale for currents is used.

+ABS

$ Initial bias point at -50 V

SOLVE V (BACK_CONTACT) =0 ELEC= BACK_CONTACT

SOLVE V (FRONT_CONTACT) = -50 ELEC= FRONT_CONTACT

$ Code to simulate I-V from -50 to + 50 V in steps of 1 V

Appendix I (Continued)

PHOTOGEN RAYTRACE X.ORG= 150 Y.ORG= -5 WAVE.LENG=0.57 FLUX=1E15

SOLVE ELEC= FRONT_CONTACT VSTEP=1 NSTEP=100